Meteorologische Zeitschrift, PrePub DOI 10.1127/metz/2016/0780

Numerical simulations of homogeneously nucleated natural cirrus and contrail-cirrus. Part 2: Interaction on local scale

Simon Unterstrasser*, Klaus Gierens, Ingo Sölch and Martin Wirth

Deutsches Zentrum für Luft- und Raumfahrt (DLR) – Institut für Physik der Atmosphäre, Oberpfaffenhofen, Germany

(Manuscript received January 29, 2016; in revised form May 12, 2016; accepted June 17, 2016)

Abstract

The interaction of contrail-cirrus and natural cirrus formed by homogeneous nucleation is studied over up to ten hours by means of a LES model equipped with a Lagrangian ice microphysics module. A pre-existing contrail evolves in an ascending air mass and becomes surrounded by natural cirrus. Such scenarios are compared to scenarios, where the ascent stops, before natural cirrus formation sets in. It is found that in high updraught cases contrail spreading is inhibited by surrounding cirrus and contrail total extinction is strongly reduced. In a slow updraught the cirrus forms later around a mature contrail and the contrail's further evolution is not considerably perturbed by the cirrus. Analysing the simulated extinction coefficient of such a dual-origin ice cloud suggests that contrails becoming embedded in cirrus do not generally remain identifiable as such in observations. It is further demonstrated that cirrus ice crystals exist in large parts of the contrail. If the contrail is located in the middle of a moist layer and the surrounding cirrus, it can happen that the complete contrail is "contaminated" with cirrus ice crystals within several hours. Finally, contrail properties are computed with and without considering the co-existing cirrus ice crystals which aids the interpretation of potentially "contaminated" contrail observations.

Keywords: Large eddy simulation, Lagrangian ice microphysics, Natural cirrus, contrail cirrus, aviation

1 Introduction

Contrail-cirrus are probably the largest aviation contribution to climate change in terms of radiative forcing (Burkhardt and Kärcher, 2011). Process-based numerical simulations can deepen process understanding and eventually help reducing the uncertainties associated with such climate estimates. In a companion paper (Unterstrasser et al., 2016) separate simulations of both contrails and cirrus were presented. Those simulations helped clarifying how different both cloud types are and whether it is possible to deduce microphysical criteria that allow distinguishing contrails from cirrus in observations. In the present study, the focus is on the interaction of both cloud types, that is, when a pre-existing contrail becomes embedded in natural cirrus. The impact of a surrounding cirrus on contrail evolution is analysed first with regard to integral contrail properties. These are then compared to scenarios where no cirrus clouds form. Whether a contrail remains identifiable as such after it got embedded into cirrus is discussed. Parts of the contrail eventually become seeded with crystals from the surrounding cirrus, which might be considered "contamination". How such contamination modifies local contrail properties, is discussed as well and aids the interpretation of potentially "contaminated" contrail observations.

To simplify the description of our simulation results we refer to cirrus if we speak of a naturally formed cirrus. The term contrail refers both to linear contrails and aged contrails where the term contrail-cirrus would be more appropriate. Conveniently, this circumvents the need to distinguish between contrail and contrail-cirrus. The neutral term ice cloud is used, if the cloud type is unspecified or if it is a mix of both cloud types.

This paper is organised as follows. Section 2 presents the methods and introduces the employed model together with the design of the numerical set-up. Simulations of interacting contrails and cirrus are described in Section 3. The simulation results are analysed in Section 4, namely the aspect of contrail identification in Section 4.1, the mixing of both cloud types (contamination of the contrail with cirrus crystals) in the Section 4.2, and finally, how much this contamination affects local contrail properties in Section 4.3. Further discussion is given in Section 5 and conclusions are drawn in the final Section 6.

2 Methods

This section introduces the employed model and the numerical set-up. Quantities that will be used in the later analysis have been defined in PART 1 (Unterstrasser et al., 2016). These definitions will not be repeated here.

2.1 Model description

The numerical simulations have been carried out with the non-hydrostatic anelastic model EULAG (Smo-

*Corresponding author: Simon Unterstrasser, DLR Oberpfaffenhofen, 82234 Wessling, Germany, e-mail: simon.unterstrasser@dlr.de

larkiewicz and Margolin, 1997) which employs the positive definite advection scheme MPDATA (Smolarkiewicz and Margolin, 1998) in its Eulerian operation mode. A microphysical module using Lagrangian tracking of ice crystals (Sölch and Kärcher, 2010) is fully coupled to EULAG and forms the version EULAG-LCM. With this model version the simulation of both natural cirrus and contrails is possible. Recent examples are studies of a mid-latitude cirrus cloud system with special focus on aggregation (Sölch and Kärcher, 2011) and contrail evolution during the vortex phase (Unterstrasser, 2014; Unterstrasser and Görsch, 2014).

The microphysical module LCM uses an explicit representation of size-resolved non-equilibrium aerosol and ice microphysics. Ice crystals (IC) are represented in the model by Lagrangian simulation particles (SIPs). Every SIP represents a large number of ICs with identical properties, and the actual number of SIPs as well as the number of ICs a SIP represents vary dynamically during a run of the model (Unterstrasser and Sölch, 2014). In its complete form the LCM comprises non-equilibrium growth of liquid supercooled aerosol particles, their homogeneous freezing, heterogeneous nucleation of ice nuclei in the deposition or immersion mode, growth of ICs by deposition of water vapour (WV), their gravitational sedimentation, aggregation between ICs due to differential sedimentation, turbulent dispersion of ICs, latent heat release, and radiative impact on particle growth. Not all of these processes are switched on in the present simulations in order to reduce the complexity of the situations. Heterogeneous nucleation, aggregation and radiation are deactivated, although they can strongly alter the evolution of cirrus and contrails (e.g. Dobbie and Jonas, 2001; Liu et al., 2003; Spichtinger and Gierens, 2009a; Unterstrasser and Gierens, 2010b; Sölch and Kärcher, 2011; Lewellen, 2014).

The information contained in the SIPs is mapped on the Eulerian grid, which is used for all non-ice variables. For instance, the IC number concentration n in a grid point is computed by summing up the number of ICs represented by each SIP belonging to this grid box and dividing the sum by the volume of the grid box.

The subgrid turbulence model uses the TKE-approach. Synoptic scale updraught motion is prescribed via an external forcing term in the temperature equation in order to accommodate for the adiabatic temperature change. Details of the implementation can be found in Unterstrasser and Gierens (2010b).

The data structure of the SIPs was extended such that the origin of each SIP, i.e. the mechanism by which the ICs formed (contrail or cirrus), is saved. Compared to Eulerian approaches, where a second instance of prognostic variables had to be introduced, this separation feature comes at virtually no extra computational cost (CPU time and storage) in our Lagrangian approach. This greatly enhances the analysis capabilities, e.g. separate contrail and cirrus size distributions can be computed offline. Moreover, regions of co-existing contrail and cirrus ICs can be identified and analyses can be confined to this region.

2.2 Simulation set-up

The simulation set-up used in this study has already been introduced in Unterstrasser et al. (2016, denoted as INTERACTION simulation) but will be repeated here. A $L_x = 40\,\mathrm{km}$ times $L_z = 3\,\mathrm{km}$ domain with a resolution of 10 m in each direction is used. A 5 minute old contrail, about 500 m deep and 200 m broad and provided by a 3D simulation of a young contrail (Unterstrasser, 2014), served as starting point. It consists of about $\mathcal{N}_0 = 1.7 \cdot 10^{12}$ ICs (per flight meter) corresponding to an IC 'emission' index of $2.8 \cdot 10^{14}(\mathrm{kg\ fuel})^{-1}$ and roughly half of the ICs surviving the vortex phase. Unlike to the contrail simulations shown in PART1 (Unterstrasser et al., 2016), homogeneous nucleation is switched on and cirrus forms around the contrail once the relative humidity RH_i surpasses the critical humidity threshold. The cruise altitude of the contrail generating aircraft is at temperature $T_{CA} = 217\,\mathrm{K}$, which corresponds to typical upper tropospheric conditions, and is located at $z_{CA} = 2000\,\mathrm{m}$ above the bottom of the simulation domain.

In the default case, the contrail forms slightly below the top of an ice-supersaturated (ISS) layer, which is around $d_{ISSR} = 1200\,\mathrm{m}$ deep. Distances $d_{up} = 100\,\mathrm{m}$ and $d_{down} = 1100\,\mathrm{m}$ lie above and below the contrail formation altitude in the ISS layer, respectively. Thus, the top of the emerging cirrus and the contrail core region eventually occupy similar altitudes. In a sensitivity study the ISS layer is shifted upwards by 500 m, implying $d_{up} = d_{down} = 600\,\mathrm{m}$. Then, the contrail lies in the middle of the ISS layer and of the emerging cirrus. Due to the upward shift, the ISS layer and the cirrus are cooler by around 3 K–4 K. As z_{CA} is unchanged, contrail formation occurs at 217 K in both scenarios. Both humidity profiles are depicted in Figure 1 bottom.

In Unterstrasser et al. (2016) contrails were simulated in atmospheric situations where ambient relative humidity RH_i^* rose from 120 % to around 150 % (corresponding to an adiabatic cooling of 2 K). For such a scenario it was reasonable to assume that natural cirrus formation by homogeneous nucleation does not happen since the nucleation threshold was not reached. Now a longer updraught is prescribed with final adiabatic cooling of 4 K where ambient relative humidity would rise from 120 % to 190 % (or, equivalently supersaturation would rise from $s_{init} = 0.2$ to $s_{final} = 0.9$, with supersaturation $s = RH_i - 1$ with respect to ice). Then, natural cirrus will form around the pre-existing contrail once the nucleation threshold $RH_{crit} \approx 150\,\%$ is reached and surpassed. Depending on the updraught speed w_{syn}, the natural cirrus forms at different contrail ages (see vertical lines in Figure 4). The time of cirrus formation in the 4 K-cases is similar to the time the updraught comes to a halt in the 2 K-cases of PART1 (Unterstrasser et al., 2016). The temporal evolution of ambient relative hu-

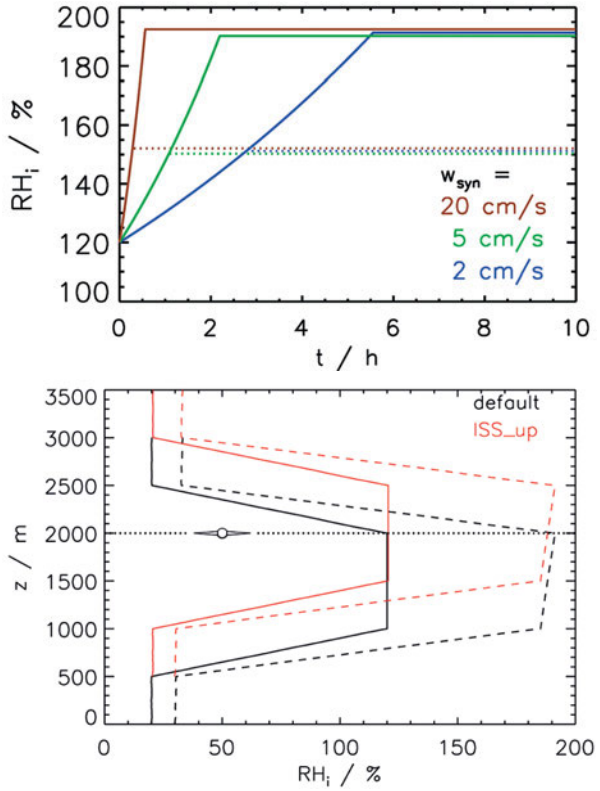

Figure 1: top: Temporal evolution of relative humidity $RH_i^*(t)$ at $z = 2000$ m for updraught speeds $w_{syn} = 2\,\mathrm{cm\,s^{-1}}$ (blue), $5\,\mathrm{cm\,s^{-1}}$ (green) and $20\,\mathrm{cm\,s^{-1}}$ (brown). The final adiabatic cooling is either 2 K (dotted) or 4 K (solid). bottom: vertical profile of RH_i^* in the beginning (solid) and after an adiabatic cooling by 4 K (dashed). The flight altitude of the contrail-producing aircraft is at $z_{CA} = 2000$ m. The black lines show the standard case with the contrail at the top of the ice-supersaturated (ISS) layer ('default'). The red lines show the case, where the ISS layer is shifted upwards by 500 m ('ISS_up').

midity is shown in Figure 1 top. Cases with $w_{syn} = 20$, 5 and $2\,\mathrm{cm\,s^{-1}}$ are treated.

The initial contrail is represented by around 10^6 SIPs. To increase computational efficiency, several numerical improvements have been introduced in LCM to optimise the number of SIPs used (Unterstrasser and Sölch, 2014). A splitting technique is periodically applied to contrail SIPs in order to maintain sufficiently high SIP concentrations in the diluting contrail. The natural cirrus is represented by up to $35 \cdot 10^6$ SIPs. By employing a stochastic nucleation implementation and a SIP merging technique, the SIP number could be considerably reduced compared to earlier simulations.

Table 2 summarises important simulation parameters.

3 Interaction between contrail and cirrus

3.1 Theoretical considerations

Before the interaction between contrail and cirrus will be discussed, the basic mechanisms of contrail growth in the absence of cirrus formation are repeated.

Table 1: Characteristics of the various updraught scenarios: updraught speed w_{syn}, updraught duration $t_{updr,2K}$ and $t_{updr,4K}$ for a 2 K or 4 K cooling, respectively and the approximate time of cirrus formation t_{nuc}. The right-most column indicates the colours used in several plots throughout the paper.

w_{syn} in $\mathrm{cm\,s^{-1}}$	$t_{updr,2K}$ in s	$t_{updr,4K}$ in s	t_{nuc} in %	colour
2	10000	20000	10200	blue
5	4000	8000	4000	green
20	1000	2000	1000	brown

Table 2: Parameters of the simulation set-up: temperature at cruise altitude T_{CA}, Brunt-Väisälä frequency N_{BV}, initial relative humidity RH_i, depth of ice-supersaturated (ISS) layer d_{ISSR}, root-mean square of initial turbulent velocity fluctuations $\hat{u}$, vertical wind shear du/dz, initial number of ice crystals in the contrail $\mathcal{N}_0$, depth of ISS layer above/below cruise altitude d_{up}/d_{down}.

T_{CA}	217 K	N_{BV}	$10^{-2}\,\mathrm{s^{-1}}$
$RH_{i,init}$	120 %	d_{ISSR}	1200 m
$\hat{u}$	$0.12\,\mathrm{m\,s^{-1}}$	du/dz	$0.002\,\mathrm{s^{-1}}$
$\mathcal{N}_0$	$1.7 \cdot 10^{12}\,\mathrm{m^{-1}}$		
	default		ISS_up
d_{up}	100 m	d_{up}	600 m
d_{down}	1100 m	d_{down}	600 m

Following Lewellen (2014) and Unterstrasser and Gierens (2010a) it is reasonable to divide the contrail into two distinct parts:

1. The contrail core has high concentrations of small ICs whose bulk settling velocity is very small (say, mm/s)

2. The fall streak has fewer, yet larger ICs with considerable settling velocities.

Even though the fall streak usually covers a larger area than the core, the total IC number of that part constitutes only a small fraction of the total population. Four types of growth mechanisms can be identified for the ice crystals in a contrail:

- mechanism G1: growth of ice crystals in the contrail core
- mechanism G2: growth of ice crystals at the periphery of the contrail (core), mainly due to entrainment of moisture from supersaturated air by horizontal mixing
- mechanism G3: growth of ice crystals falling into a moist, so far ice crystal free, area below the contrail
- mechanism G4: growth of ice crystals within the fall streak

The essential difference between G3 and G4 is that a cirrus can form in the G3-region, but not in the G4-region, where RH_i is usually kept below the nucleation threshold RH_{crit} due to contrail ICs. Figure 2 (left) schematically illustrates the various growth processes in the absence of cirrus.

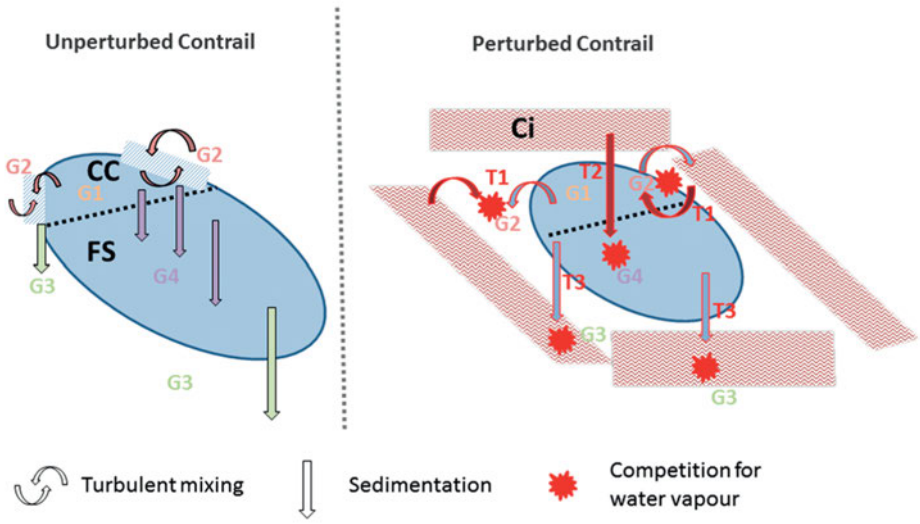

Figure 2: Schematic illustration of the growth processes of a contrail in the absence of cirrus (left) and with surrounding cirrus (right). CC, FS and Ci denote the contrail core, the contrail fall streak and the cirrus, respectively. G1-G4 denote various growth processes and T1-T3 transport processes that lead to the co-existence of contrail and cirrus crystals and competition for the available water vapour (red blobs). See text for more information.

We introduce a deposition timescale as

$$\tau_g = \left| \frac{e - e^*}{de/dt} \right| \tag{3.1}$$

with vapour pressure e and vapour pressure at ice saturation e^*. Following Gierens (2003, Eq. 18), $\tau_g \propto n^{-2/3} s^{-1/3}$. Following Eq. 19 of the latter publication, an updraught time scale can be defined as

$$\left(\frac{\tau_u}{\mathrm{s}}\right) = \frac{1}{60}\left(\frac{T}{\mathrm{K}}\right)^2 \left(\frac{w_{syn}}{\mathrm{m/s}}\right)^{-1} \tag{3.2}$$

which quantifies the supersaturation change due to adiabatic cooling in an ascending air parcel. In the present simulations, the updraught time scale ranges from one to ten hours. To quantify the combined effect of deposition and updraught on the supersaturation evolution, a supersaturation timescale τ_s is introduced. From Eq. 11 of the latter publication follows:

$$\tau_s{}^{-1} = \tau_g{}^{-1} - \tau_u{}^{-1} \tag{3.3}$$

In the following, the focus is on situations in mature clouds, where s decreases, i.e. $\tau_g < \tau_u$ and $\tau_s > 0$ is guaranteed. In such an idealised competition, supersaturation converges to the asymptotic limit $\tilde{s} = \tau_s/\tau_u$. At this point, τ_g approaches $\tau_u\, \tilde{s}/(1+\tilde{s})$.

In the contrail core, relative humidity is quickly relaxed to saturation (see Figure 13 of PART1, Unterstrasser et al., 2016) as $\tau_{g,Core} \ll \tau_u$. After this growth period, which typically lasts not longer than a few minutes because of the high IC number concentrations, the supersaturation is consumed and $s \to \tilde{s}_{core}$ very close to 0. From then on, only the updraught time scale remains important, as it measures how much WV becomes available per unit time and controls the further growth of ICs in the contrail core, G1. ICs in the contrail core grow only as long as an ascent prevails. Mechanism G2 was identified to trigger the formation of the fall streaks (Heymsfield et al., 1998). Few ICs at the periphery grow (G2) and start to precipitate into the undepleted environment below where they continue their growth (G3). Lewellen et al. (2014) coined the term precipitation instability for this process. In the fall streaks, number concentrations are low, $\tau_{g,\mathrm{Falls}}$ and $\tau_{s,\mathrm{Falls}}$ are large and excess WV is slowly depleted and $\tilde{s}_{FS}$ is higher than $\tilde{s}_{core}$. Hence, the precipitating ICs do not necessarily have to fall into new crystal-free areas; they can continue their growth also inside the fall streaks (G4). There, IC growth usually continues beyond the point where the ascent comes to a halt. In contrast to the contrail core, its growth rate can be decoupled from τ_u.

Next the effect of cirrus on the contrail evolution is discussed. The time span, t_{age}, defines the period between contrail formation and cirrus formation. It follows

$$t_{age} \propto \frac{s_{crit} - s_{init}}{w_{syn}}, \tag{3.4}$$

where s_{init} is the ambient supersaturation at contrail formation. The closer s_{init} is to the nucleation threshold s_{crit} and the higher w_{syn} is, the earlier cirrus forms.

The maximum amount of WV, M_{dep} that is eventually available for deposition depends on:

$$M_{dep} \propto t_{updr} w_{syn} \propto s_{final} \tag{3.5}$$

This mass is distributed among the two populations in different shares. Details depend on the magnitude of the involved time-scales.

Once contrail and cirrus ICs share the same space (how this happens is explained later), they compete for

the available WV. Of course, depletion of WV is accelerated once two populations of ICs contribute since $\tau_g(n_1 + n_2) < \tau_g(n_1)$ and $\tau_g(n_2)$. However, each population grows less in the presence of the other one. But, how is the deposited WV distributed among the two populations? The mass growth of a single IC can be cast into the form (Koenig, 1971; Spichtinger and Gierens, 2009b)

$$\frac{dm}{dt} = am^b \tag{3.6}$$

and the mass growth of a population with a certain mass distribution is proportional to the moment of order b ($\approx 1/3$, see Figure 4 of Spichtinger and Gierens, 2009b). The moment of order b is in turn proportional to $\bar{m}^b$ (with mean mass $\bar{m}$), such that the growth of the total mass $M = n\bar{m}$ is approximately proportional to $n\bar{m}^b$. The relative growth of two populations is then simply given by

$$\frac{dM_1/dt}{dM_2/dt} = \left(\frac{\bar{m}_1}{\bar{m}_2}\right)^b \left(\frac{n_1}{n_2}\right). \tag{3.7}$$

As $b \approx 1/3$, the IC mass ratio has a smaller effect than the IC number ratio. If corresponding sizes instead of IC masses had been considered, the exponent would be even smaller, of the order $1/9 \ldots 1/5$, depending on mass-size-relations of the ICs (Mitchell, 1996); thus IC size ratios are not nearly as relevant as number ratios for this consideration.

In the following, let us consider the question where cirrus can form and whether homogeneous nucleation of cirrus ICs is possible inside the contrail. In the contrail core, $s \approx 0$ after the initial growth period, and the contrail IC number concentration is too large to drive s far above 0 even if the updraught would get stronger as $\tau_{g,Core} << \tau_u$. Thus, no homogeneous nucleation is possible in the contrail core (even heterogeneous nucleation is highly improbable unless it would proceed at very low supersaturation of the order $\tilde{s}_{core}$). In the contrail fall streak, $\tau_{g,\mathrm{Falls}} \lesssim \tau_u$ in the simulations. Thus, here it is neither possible that the ongoing updraught drives the supersaturation beyond the threshold for homogeneous nucleation (heterogeneous nucleation might happen in nature, but is switched off in our simulations); cirrus forms only outside of the contrail in the present simulations.

Hence, interaction of two IC populations, here contrail and cirrus ICs, requires that both populations become mixed by transport processes so that they occupy the same space and compete for the excess WV. Three types of transport processes may lead to co-existence of contrail and cirrus ICs. These are:

- mechanism T1: Turbulent mixing at the contrail periphery
- mechanism T2: Cirrus ice crystals from above fall into the contrail
- mechanism T3: Ice crystals from the contrail fall streak fall into the cirrus underneath

Figure 2 (right) schematically illustrates the various transport processes and how the co-existence of two IC populations affects the contrail growth processes.

Mixing is not instantaneous and it takes a certain time τ_m for both IC populations to get mixed and to start to compete for the available WV. Before mixing, the initial supersaturation is locally reduced to some value s_1 by just one of the two populations at a rate $\propto \tau_g^{-1}$. After mixing, both populations compete for the remaining supersaturation s_1 plus the WV that becomes available due to adiabatic cooling. Eq. 3.7 roughly estimates the WV share each population receives. How important the competition between both cloud types is depends on an interplay of all time scales introduced so far and on the question, whether the amount of WV that deposits on ICs before mixing or the amount that both populations compete for after mixing is larger. The latter partitioning also depends on s_{init}, s_{crit} and s_{final}. Such questions can only be answered by simulations that model this interaction in detail.

The importance of the mentioned transport and interaction processes is discussed next. In the core, contrail growth is not much affected by cirrus. Cirrus ICs from above may fall into the core (T2) or mix laterally into the core (T1). Usually, $\tau_{s,Core}$ is much smaller than $t_{age} + \tau_m$, which is the time it takes the cirrus ICs to arrive in the core. Hence, the contrail ICs have enough time to deplete all excessive WV. Even, if the updraught continues beyond the point, where cirrus ICs populate the contrail core (i.e. $t_{updr} > t_{age} + \tau_m$) and additional WV becomes available, the cirrus ICs are just too few to get a substantial share of it.

At the contrail periphery turbulent mixing of both IC populations could impact the interaction. In order to test this, we compute how far a contrail can expand horizontally by turbulent diffusion within a time $\tau_{s,Ci}$, using the Einstein-Smoluchowski relation between the (turbulent) diffusion coefficient, D_{turb}, and the root mean square displacement due to diffusion, d_{rms}: $d_{rms} = (2D_{turb}\ \tau_{s,Ci})^{1/2}$. D_{turb} is of the order 10 to 20 $\mathrm{m\,s^{-2}}$, (Dürbeck and Gerz, 1995), and, if for instance $\tau_{s,Ci}$ is of the order 1000 s, then the contrail can grow another $L = 100$ m laterally until the cirrus ICs consumed the initial excessive WV. L is small compared to the typical horizontal scale of a contrail. Any further turbulent dispersion of the contrail is limited in the sense that supersaturation has been driven towards zero in the more remote parts of the cirrus and further growth of contrail ICs via G2 occurs only if the ascent continues. The aforementioned precipitation instability may be largely choked off by the cirrus. Similarly, cirrus ICs can be mixed into the contrail. In most cases, the excessive WV inside the contrail is depleted long before cirrus ICs exist or mix into the contrail. Hence, this effect is rated to be ineffective.

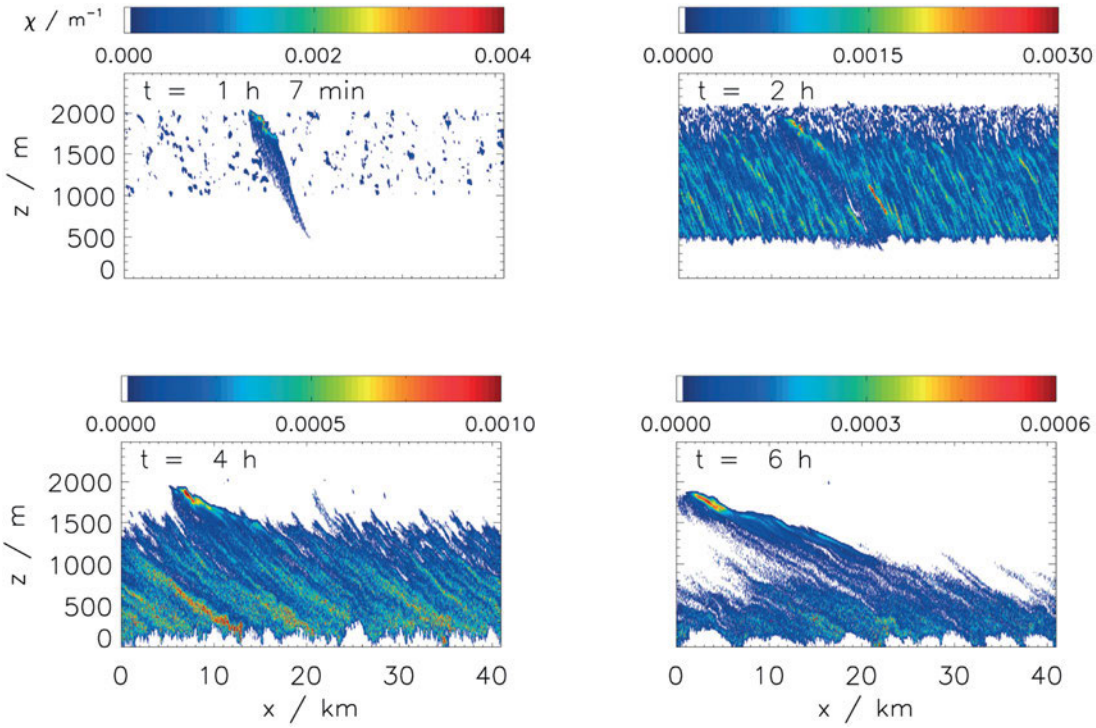

Figure 3: Extinction coefficient χ of a contrail and an emerging cirrus for the indicated simulation times and the default simulation with $w_{syn} = 5\,\mathrm{cm\,s^{-1}}$. Note the different ranges of the colour bars.

As a next step, mixing of the two populations by (differential) sedimentation is considered. It may take a time $\tau_{sed} = d_{FS}/v_{t,Ci}$ (with the depth of the fall streak, d_{FS} and the terminal velocity of the cirrus ICs, $v_{t,Ci}$) for cirrus ICs to invade the contrail fall streak down to its lower edge. Within a similar period of time, ICs of the contrail fall streak may fall into the cirrus. The simulations show that the deposition time scales in the cirrus and the contrail fall streak are at least similar if not even longer than the sedimentation time scales τ_{sed}. Then, the initial supersaturation is not yet consumed by the time both populations start to compete for the WV.

Hence, one can expect that 1.) growth in the contrail fall streak (mechanism G4) is reduced once the cirrus ICs arrive there and 2.) mechanism G3 is reduced once cirrus forms in the contrail's environment and starts to deplete the WV before the contrail ICs arrive there. In the latter case, the G3-region is not ice crystal free any longer (as stated in the original definition of G3), but populated with cirrus ICs that precede the contrail ICs.

It can also happen that cirrus ICs reduced the supersaturation in regions where they fell out by the time the contrail ICs arrive. In this case, the contrail growth is affected, even though there is no strict co-existence of both populations.

Whether these general expectations are confirmed by the simulations is analysed next.

3.2 Simulation example

In order to set the stage for further detailed discussion, an example simulation is described first, where a contrail spreads in an ascending air mass which at some point allows for cirrus formation by homogeneous nucleation in the surrounding air. Figure 3 shows a contour plot of the IC extinction coefficient χ, which is proportional to the surface area of the ICs per unit volume. In the remainder of this text, we refer to χ simply as extinction. The extinction increases for increasing ice water content IWC and number concentration n. About one hour after its formation at $t = 0\,\mathrm{h}$, the contrail is moderately tilted due to vertical wind shear and a fall streak is evident with the lowest ICs penetrating into the subsaturated layer below approximately $z = 800\,\mathrm{m}$. Even though the mean relative humidity in the ISS layer is still below the nucleation threshold in the example with $w_{syn} = 5\,\mathrm{cm\,s^{-1}}$, turbulent fluctuations generated spots where the nucleation threshold was already surpassed and cirrus ICs are present. After two hours nucleation occurred across the complete ISS layer. At that time the presence of a contrail inside the cirrus is not obvious. Contrail spreading is apparently inhibited by the surrounding cirrus. In the cloud top region there are IC-free areas where crystal growth has reduced supersaturation to values below the nucleation threshold. Nucleation thus ceased and the ICs already fell out of this layer due to sedimentation, leaving a cloud free volume behind. The ascent of the air mass and the corresponding increase of RH_i stop after around 2 h 15 min and formation of ICs soon ceases. After four hours the effect of sedimentation is apparent, as the cirrus top level sank from $z = 2000\,\mathrm{m}$ down to $z = 1500\,\mathrm{m}$. In contrast, the contrail core with its many small ICs still resides around its initial altitude. After 6 hours, the cirrus is about to decay and confined to the lowest part

of the domain. This layer was initially strongly subsaturated, but became hydrated over time by sublimating ICs and now contains the remnants of the cirrus. The contrail, then again, conserved high extinction values in its core which is only 200 m below the original formation altitude. Compared to a contrail which has not become surrounded by cirrus (Unterstrasser et al., 2016), the tilted contrail is thinner and covers a smaller area. This is due to the fact that mechanism G2 is not as effective and hence contrail expansion by sedimentation is smaller. In this example, the contrail lifetime is larger than the cirrus lifetime. The latter depends strongly on the updraught speed as seen in PART 1. (Unterstrasser et al., 2016)

3.3 Contrail evolution under the influence of a surrounding cirrus

The evolution of a contrail under the influence of a surrounding cirrus is discussed in this section. By varying the depths d_{down} and d_{up} of the ISS layer below/above the contrail and updraught speed w_{syn}, various ambient scenarios are prescribed. These variations affect the cirrus as well as the contrail properties. According to the design of our scenarios, the implications of such variations on the interaction between contrail and cirrus are twofold: The stronger the updraught is,

1. the earlier the cirrus forms and the less time the contrail has to spread freely and
2. the higher n_{Ci}, the longer the cirrus lifetime and the smaller $\tau_{g,Ci}$.

All these sensitivity studies are performed for both, contrails in clear sky (*unperturbed* contrail, the uplift stops after a cooling of 2 K) and contrails becoming embedded in cirrus clouds (*perturbed* contrail, the uplift stops after a cooling of 4 K). With a total cooling of 4 K, contrail growth in the perturbed cases via G1 is more substantial than in the corresponding unperturbed cases. In turn, the presence of a cirrus would reduce the strength of G2 and G3. These implications of a surrounding cirrus for the growth mechanisms will be signified in the following with simple symbols, for instance G1 $\uparrow$, G2 $\downarrow$ and G3 $\downarrow$ for the impacts just discussed. The impact of a cirrus on G4 is not as easily predicted because enhancing (more excess WV) and weakening effects (smaller fall streak) are present simultaneously.

Figure 4 displays the temporal development of total extinction, effective diameter and total crystal number (per metre of flight path) for perturbed (solid lines) and unperturbed (dotted lines) contrails in situations with contrail formation at the top (left column) and in the middle (right column) of the supersaturated layer. Total extinction E is a metric for the (radiative) significance of an individual contrail. Note that in the perturbed cases too, the displayed quantities refer only to the contrail, not to the whole ice cloud. Different colours refer to different updraught speeds. For $w_{syn} = 20\,\mathrm{cm\,s^{-1}}$ (brown curves), the cirrus forms at a contrail age of 20 minutes and contrail spreading is strongly inhibited. The total extinction of the perturbed contrail is several times smaller than that of the unperturbed contrail. For this fast uplift cirrus formation causes the strength of mechanisms G2, G3 and G4 to decrease more than that of mechanism G1 to increase (i.e. in our simple symbols: G2 $\downarrow$ + G3 $\downarrow$ + G4 $\downarrow$ > G1 $\uparrow$).

For a weaker updraught of $w_{syn} = 5\,\mathrm{cm\,s^{-1}}$, the cirrus forms about one hour later and the contrail already covers a larger area. In this case, E of the perturbed contrail is only slightly smaller than that of the unperturbed contrail (implying G2 $\downarrow$ + G3 $\downarrow$ + G4 $\downarrow \gtrsim$ G1 $\uparrow$). The increase of E gets weaker in both cases after one hour; in the perturbed case due to the cirrus, which diminishes G2, G3, G4, and in the unperturbed case because the uplift ceases, which immediately stops G1 in the contrail core and gradually decreases G4 down to zero.

In the case with the weakest considered uplift, $w_{syn} = 2\,\mathrm{cm\,s^{-1}}$, the contrail spreads for almost three hours before the cirrus forms. Opposite to the latter two cases, the perturbed contrail has a higher total extinction than the unperturbed one (i.e. G2 $\downarrow$+G3 $\downarrow$ < G1 $\uparrow$+G4 $\uparrow$). E of the perturbed contrail rises over the whole updraught period and drops quickly once the ascent stops after around six hours. This demonstrates the strong dependence of G1 on the current cooling rate.

In the ISS_up sensitivity simulations (see right column of Figure 4) contrail formation occurs in the middle of the ISS layer. The smaller distance to the lower end of the supersaturated layer leads to smaller fall streaks than in the default case. This leads to lower E-values in the unperturbed contrails since $d_{down}\downarrow \Rightarrow$ G3 $\downarrow$ + G4 $\downarrow$. The effect of a surrounding cirrus on contrails in the middle of the supersaturated layer is smaller, but qualitatively similar to the default case with the contrail at the top of the ISS layer.

The evolution of the effective diameter is shown in the middle row of Figure 4. Common to all unperturbed contrails is the pattern of an initial growth followed by a period of quasi-constant D_{eff}-values. In the default case (contrail formation close to the top of the ISS layer), values of 50 µm–60 µm are reached compared to $\lesssim$ 40 µm in the ISS_up simulations. Earlier simulation studies using $d_{down} = 1100$ m showed no dependence of these quasi-constant effective diameters on updraught speed and final adiabatic cooling (Unterstrasser et al., 2016), nor on aircraft type (Unterstrasser and Görsch, 2014). The ISS_up simulations suggest that d_{down} is the dominant parameter for the D_{eff}-evolution. This will become clearer by an analysis of crystal size distributions (given below).

Values of D_{eff} are generally smaller in a perturbed than in an unperturbed contrail. The earlier the cirrus forms, the smaller the contrail fall streak is. In these cases, $d_{FS} < d_{down}$. Then, the contribution of the small ICs in the contrail core dominates over that of the large ICs in the fall streak in the computation of D_{eff}. Hence, D_{eff} starts to decrease, once cirrus forms

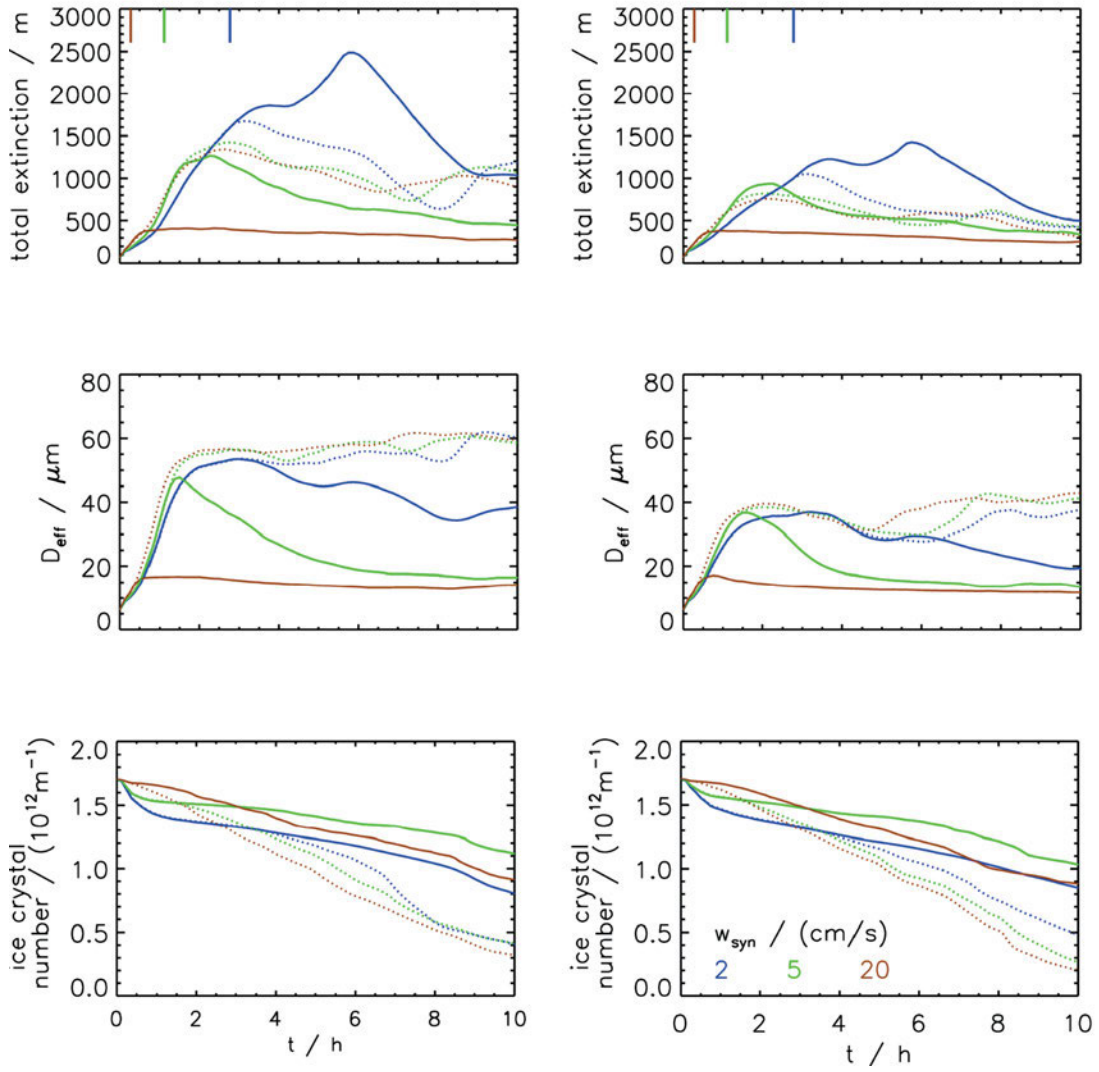

Figure 4: Temporal evolution of various contrail properties for various updraught speeds (for colour codes see Table 1 or legend in bottom right panel): total extinction E, effective diameter D_{eff} and ice crystal number $\mathcal{N}$ (from top to bottom). Solid lines: scenario with surrounding cirrus and $\Delta T_{final} = 4$ K; dotted lines: scenario without cirrus and $\Delta T_{final} = 2$ K.
Left column shows the default simulations and the right column the ISS_up simulations. The vertical bars indicate, on the one hand, the onset of cirrus formation in the 4 K-simulations and, on the other hand, the stop of the updraught in the 2 K-simulations.

($w_{syn} = 2\,\mathrm{cm\,s^{-1}}$ or $5\,\mathrm{cm\,s^{-1}}$) or D_{eff} remains small right from the beginning ($w_{syn} = 20\,\mathrm{cm\,s^{-1}}$).

Figure 4 bottom shows the evolution of IC number $\mathcal{N}$. Surprisingly at first glance, the crystal loss is smaller if a contrail is perturbed by surrounding cirrus. However, this effect can be easily explained: the presence of the cirrus chokes off of the precipitation instability which otherwise (in clear sky) would lead to larger contrail ICs via growth mechanisms G2 and G3. Notably, the differences between the default and ISS_up-set-up are very small.

Figure 5 shows IC size distributions (SD) of 4 hour old contrails. All SDs have a characteristic shape with a strong peak at small IC sizes and a second mode with larger ICs. The prominence of the second mode depends on the simulation scenario. Large ICs are generally less abundant, when the formation of a strong contrail fall streak is hampered, either by cirrus formation below the contrail (solid vs. dotted curves) or a shallower ISS layer below the contrail (right vs. left panel). For a $d_{down} = 1100$ m thick ISS layer below the contrail (left panel), the maximum IC sizes are well above 200 µm, whereas for a shallower ISS layer ($d_{down} = 600$ m; right panel) L is well below 200 µm. If cirrus forms shortly after the contrail generation (i.e. the updraught is strong and t_{age} is small), ICs are usually smaller than around 100 µm. In the slow updraught case, cirrus formation sets in at a time, where the contrail has already developed a mature fall streak. In this case, the IC sizes are similar to the unperturbed case.

3.4 Further sensitivity studies

The evolution of a contrail that is embedded within a cirrus may be effected by further circumstances, e.g. the thickness of the ISS layer and vertical wind shear, to

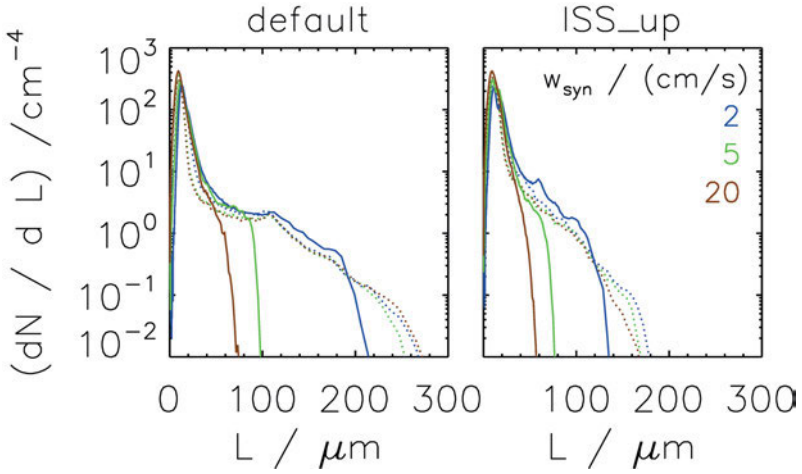

Figure 5: Ice crystal size distributions of 4 h old contrails for various updraught speeds w_{syn} (colour coding see Table 1 or legend in right panel). The left panel shows the default simulations, the right panel the ISS_up simulations. Solid lines: scenario with surrounding cirrus and $\Delta T_{final} = 4$ K; dotted lines: scenario without cirrus and $\Delta T_{final} = 2$ K.

name only two. These circumstances are considered in the following.

Assuming a shallower ISS layer with $d_{down} = 600$ m and $d_{up} = 100$ m, the ISS layer below the contrail is as thick as in the ISS_up-configuration from above, but the smaller d_{up} results in a thinner cirrus deck above the contrail. It seems that this difference is not so important: both the unperturbed and the perturbed contrails evolve very similarly to their corresponding counterparts in the ISS_up set-up (not shown). This demonstrates again the importance of d_{down} for the contrail evolution while the influence of the thickness of the cirrus layer above the contrail is of minor importance. The latter might have had a larger effect if we had allowed aggregation or radiative heating which may induce contrail lifting (Lewellen, 2014; Unterstrasser and Gierens, 2010b).

In clear sky, contrail width and total extinction increase with increasing vertical wind shear (cf. Unterstrasser et al., 2016). The higher the wind shear, the faster the contrail core and fall streak become laterally displaced. Hence, the curtain of ICs that sediment out of the core is broader, i.e. the ICs have access to more ambient WV ($du/dz\uparrow \Rightarrow$ G2$\uparrow$). Thus the cross sectional area of a contrail at the time of cirrus formation increases with increasing wind shear. From this one could expect that after cirrus formation the growth by G4 is substantial and balances the reductions of G2 and G3. However, the opposite trend is found in the sensitivity study. Contrail evolution in terms of total extinction is more strongly constrained with high wind shear ($du/dz = 0.006\,\mathrm{s}^{-1}$ with $w_{syn} = 5\,\mathrm{cm\,s}^{-1}$) than with low wind shear ($du/dz = 0.002\,\mathrm{s}^{-1}$); E decreases substantially after cirrus formation. A possible explanation is that cirrus ICs can mix more efficiently into the contrail once wind shear has led to strong tilt and elongation of the contrail. Moreover, the lateral displacement of contrail core and fall streak leads to the situation that the ICs of the core more likely fall into the surrounding cirrus than in its own fall streak, i.e. G2 is strongly reduced compared to the unperturbed case.

3.5 Effects of the lag between contrail and cirrus formation

So far, the uplift speed determined the time lag between contrail and cirrus formation, and since contrails can evolve unperturbed before cirrus appears, the volume it occupies at the time of cirrus formation is the larger the slower the uplift proceeds. Thus varying w_{syn} has two effects, it determines the duration of unperturbed contrail development but also the crystal number concentration of the cirrus that eventually impacts on the contrail. If it could be achieved that cirrus forms in the simulations with a time lag that is independent of w_{syn}, the time lag effect could be separated from the crystal number effect.

This is achieved by a retarded onset of the uplift in the $w_{syn} = 5\,\mathrm{cm\,s}^{-1}$ and $20\,\mathrm{cm\,s}^{-1}$-simulations such that cirrus forms at a contrail age similar to that of the $w_{syn} = 2\,\mathrm{cm\,s}^{-1}$-case. This is simply done by letting the uplift start at a certain contrail age (6300 s and 9100 s, respectively). Before the updraught starts, the background RH_i is held constant at 120 %. Then the cirrus forms at around $t = 10200$ s in all three cases.

Initially, total extinction increases slower as in the original simulations, as less WV is available. Once the ascent starts, total extinction rises quickly because WV becomes available at a high rate over a large contrail area and moreover it continues beyond the point of cirrus formation. Eventually, the attained peak values of E, D_{eff} and $\mathcal{N}$ are similar to the $w_{syn} = 2\,\mathrm{cm\,s}^{-1}$-case and much higher than in the original simulations with $w_{syn} = 5\,\mathrm{cm\,s}^{-1}$ and $20\,\mathrm{cm\,s}^{-1}$. This suggests that the age of the contrail at the time of cirrus formation, t_{age}, is of crucial importance for contrail properties. The subsequent competition for excess WV does not seem to be overly sensitive to the actual cirrus crystal concentration. In particular, mechanism G4 is the more important

the later the cirrus forms and the larger the contrail fall streak is at that time. A similar conclusion can be drawn when cirrus formation in the $w_{syn} = 2\,\mathrm{cm\,s^{-1}}$-cirrus is forced to proceed earlier by first prescribing a fast updraught until RH_i is closely below the nucleation threshold and then switching back to $w_{syn} = 2\,\mathrm{cm\,s^{-1}}$. In this case, the total extinction is smaller than in the original simulation with $w_{syn} = 2\,\mathrm{cm\,s^{-1}}$.

4 On the co-existence of contrails and cirrus clouds

Once cirrus clouds form in a region previously occupied by contrails alone, there is a more or less intimate co-existence of ICs from both origins. Of course one would like to know whether there is anthropogenic influence on ice clouds of unknown origin (cf. questions listed in PART1, Unterstrasser et al., 2016). Several issues become relevant in such interaction scenarios and give rise to the following questions:

- Q1: Is it possible to identify contrails as such once they become embedded in cirrus clouds?
- Q2: Can or should a contrail be considered a contrail after it loses its identity in a cirrus cloud?
- Q3: How does the entrainment of cirrus ICs alter the microphysical signature inside the contrail?

Concerning question Q1, a large-scale (global scale) identification of the anthropogenic influence in ice clouds is desirable. Hence, our analysis in Section 4.1 will focus on optical/radiative signatures in the simulations since they can be measured with lidars and passive sounders from satellites.

As mixing between both cloud types can blur the identity of both, it may get less and less meaningful to speak of contrails on one hand and cirrus clouds on the other hand. Instead, one may speak of an ice cloud of dual origin, with no clear separation into a natural and anthropogenic component. Fortunately, contrail and cirrus ICs can be still distinguished in numerical simulations which helps to answer question Q2. Analyses in Section 4.2 will detail how strongly contrail and cirrus are interwoven. We call this state *co-existence*.

In-situ chemical tracer measurements and soot residues in ICs can serve as indicators of the aviation impact and help to identify regions with contrails. Those methods can be employed in the framework of measurement campaigns. As cirrus ICs can be present in the sampled contrail regions, derived microphysical properties have to be interpreted with care and may not be representative of contrails that occur isolated from cirrus. Section 4.3 addresses Q3 and exemplarily analyses how co-existing cirrus ICs can affect size distributions and PDFs (probability density functions) of number concentrations that are evaluated inside contrails.

4.1 Contrail identification inside cirrus

Figure 6 shows a lidar observation of an ice cloud along a 190 km long path. It was measured on 18 Oct 2008 over central Europe with a high spectral resolution lidar WALES (Wirth et al., 2009). The backscatter data show a relatively faint cloud with low backscatter ratio (1–20, see the colour bars) over most of the area. However, some spots are present in the cloud with much higher backscatter ratio, exceeding 30 and even approaching 100 (see bottom panel). These spots resemble the tilted and elongated shapes of contrails that have been described above in context of the simulation with enhanced shear value. Thus it is conceivable that these spots are old contrails embedded in the large cirrus cloud. This view is supported by the heavy air-traffic in that region at that time. However, extreme scenarios, namely that the cloud completely consists of aged contrails or that it is of purely natural origin cannot be excluded without further information from beyond the reach of remote sensing. The simulation examples can be used to illustrate this point.

Figure 3 displays the field of simulated extinction coefficients, which serves here as a proxy for lidar backscatter ratio. After two hours the contrail is fully embedded in the cirrus cloud. Many tilted and elongated spots with enhanced extinction appear throughout the cloud which renders the identification of the contrail difficult.

The simulation shows that the contrail has indeed a higher extinction than its immediate neighbourhood, caused by its large IC number concentration (see Figure 7). However, the cirrus has large extinction values as well (more in the lower part of the cloud where the temperature and thus IWC is higher).

After four hours, the contrail appears at cloud top because the cirrus sedimented downwards, while the highest extinction values are found in the lower part of the cirrus, i.e in its fall streak. After six hours, when the cirrus has sunk even more, the contrail is visible far above the main part of the cirrus, but it is doubtful whether this patch of high extinction would actually be identified as a contrail from remote sensing data alone.

The incidental position of a contrail at the top of an ISS layer might support its later detection, when it reappears at cloud top. But when the contrail is formed in the middle of the ISS layer, it will not reappear, see Figure 8. After $t = 2\,\mathrm{h}$ and 4 h it is hardly possible to identify the contrail without prior knowledge. In particular at $t = 4\,\mathrm{h}$ many of the tilted elongated bands with enhanced extinction are present that could be easily misidentified as contrails.

With a high spectral resolution lidar it is possible to determine horizontal distributions of optical thickness, τ. It might be possible to identify contrails in such data as peak values. From the simulations just described the optical thickness can easily be computed by integrating the extinction coefficients along the vertical direction.

Its horizontal distribution is plotted in Figure 9 where contributions of the contrail to τ are displayed by dotted lines, the total optical thickness is given by the

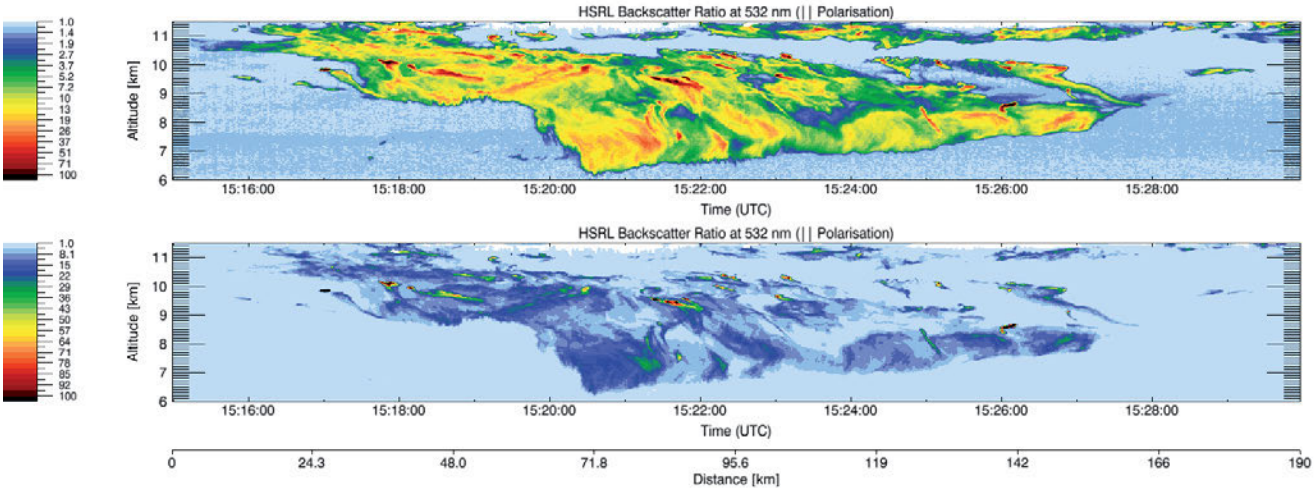

Figure 6: Lidar backscatter ratio from an airborne measurement of a cloud scene over central Europe in logarithmic scale (upper panel), the same data set in linear scale (lower panel).

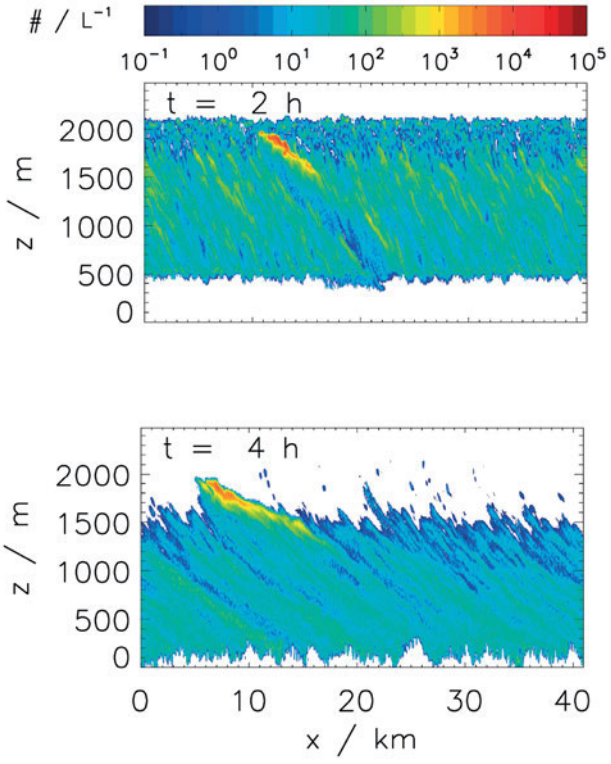

Figure 7: Number concentrations (in units L^{-1}) of a contrail and an emerging cirrus for the indicated simulation times. Same simulation as in Figure 3.

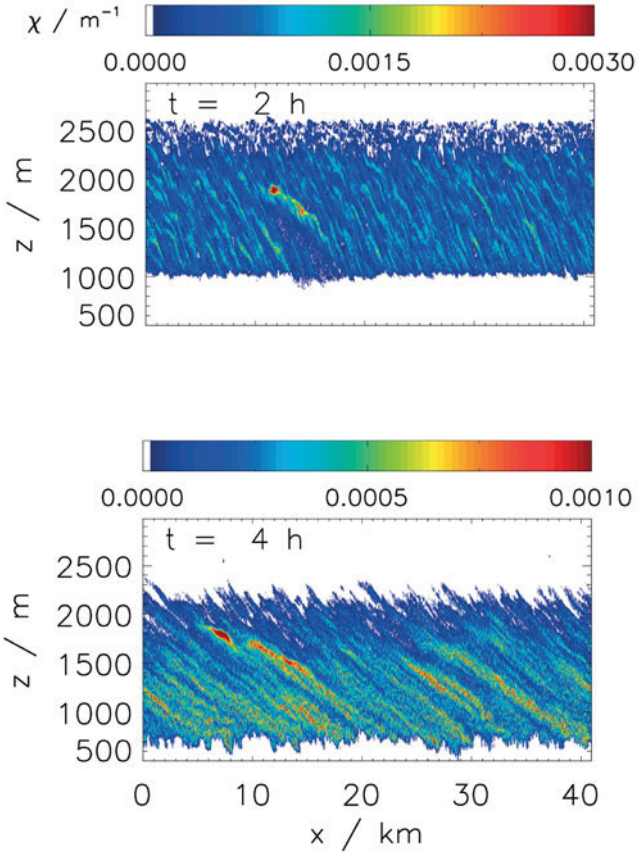

Figure 8: Extinction coefficient χ of a contrail and an emerging cirrus for the indicated simulation times and $w_{syn} = 5\,\mathrm{cm\,s^{-1}}$. Identical to Figure 3, except that the ice-supersaturated layer is shifted upwards by 500 m. Note the different ranges of the colour bars.

solid lines and different colours refer to different contrail ages.

The simulation with $w_{syn} = 5\,\mathrm{cm\,s^{-1}}$ (top row) shows no obvious contrail signal in the τ-distribution except shortly after the onset of cirrus formation ($t = 1\,\mathrm{h}\,7\,\mathrm{min}$, black curve), where the contrail peak is apparent. This young contrail could probably be identified anyway due to its line shape. Once nucleation has occurred throughout the ISS layer, τ fluctuates around 0.8. In columns where the contrail is present, it contributes with roughly 0.25 to this value. But this contribution does not appear as an addition, thus the contrail does not show up in the τ-distribution.

If the updraught is weaker ($w_{syn} = 2\,\mathrm{cm\,s^{-1}}$, bottom row), the contrail has more time to spread and develop a fall streak. After 3.5 hours nucleation just occurred

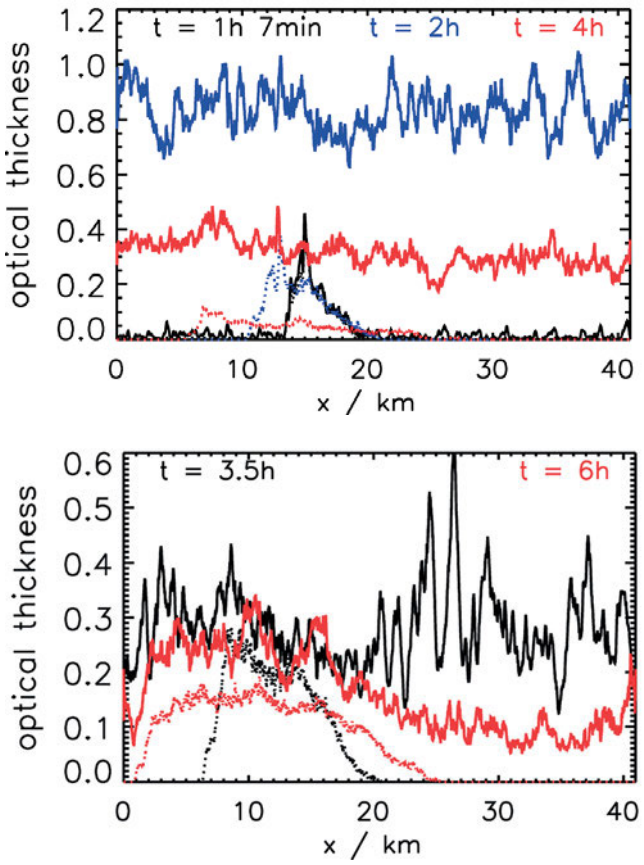

Figure 9: Horizontal distribution of optical thickness for the default simulation with $w_{syn} = 5\,\mathrm{cm\,s^{-1}}$ (top; simulation as in Figure 3) and $w_{syn} = 2\,\mathrm{cm\,s^{-1}}$ (bottom). Solid lines show the values for the total cloud (cirrus + contrail), the dotted lines show the contrail contribution. The displayed times are indicated in each panel.

across the complete ISS layer and τ reaches values of 0.35 on average. In the 'contrail' columns, the contrail ICs provide the dominant contribution to the optical thickness. But again, the local τ is not considerably higher than in the 'cirrus only' columns. The strongest peaks happen even to occur in the 'cirrus only' columns at around $x = 25$ km and, notably, τ is below its average in the region occupied by the right part of the contrail. After six hours, these relations are inverted.

For the presented simulation cases it is obvious that the contrails do not add sufficient optical thickness to the general field of optical thickness of the ice cloud to remain identifiable. Although academic homogeneous situations have been considered, the (homogeneous) background turbulence induces enough noise in the τ-distributions, that renders the detection of a contrail signal in optical thickness at least difficult. Evidently, the problem will be more difficult in realistic situations with inhomogeneous background conditions.

Independently of the identification aspect the latter case showed an example where the contrail substantially increases the radiative impact of the total ice cloud. In an upcoming study we will focus on this climate-related aspect which becomes particularly interesting when several contrails are embedded in a cirrus.

4.2 Loss of identity by co-existence

Figures 10 and 11 show the same extinction fields as in Figures 3 and 8, however now with separation of contrail (upper panels) and cirrus ICs (lower panels), respectively. The contrail area is marked by red polygons in each panel. These figures show for 2 h and 4 h old contrails how strongly ICs from both cloud types are interwoven and co-exist.

The 2 h panels of both cases show situations where parts of the contrail are still free of cirrus ICs, evident from the white patches within the red polygons in the cirrus panels. Obviously, the contrails leave holes in the cirrus, because homogeneous nucleation was suppressed in volumes with pre-existing contrail ICs.

Nevertheless, quite large fractions of the contrail areas are already populated with sedimenting cirrus ICs that form a curtain in the upper part of the contrail (mechanism T2). In the lower left corner of each contrail, it was the contrail that penetrated into the surrounding cirrus (fall streak, mechanism T3). In this region the contrail ICs are larger than the cirrus ICs. Mechanism T1 seems of minor importance in both examples, as the coexistence areas at the lateral contrail borders are small compared to the horizontal scale of the contrails.

After four hours, the complete contrail is populated with cirrus ICs in the case where the contrail is located in the middle of the ISS layer, while a segregation takes places in the case with a contrail at the top of the moist layer (caused by sedimentation of the cirrus ICs). This is quite interesting, since it means that identities get not only lost by interaction of the cloud types, but the identity can revive by later segregation of crystal types (this effect would be diminished by aggregation). Anyway, even here most of the contrail has lost its identity, mainly by mechanisms T2 and T3, less so by T1.

For a more quantitative analysis it is useful to introduce a nomenclature that simplifies the description.

The sketch in Figure 12 schematically shows the area of the pure cirrus, of the pure contrail and of their co-existence region. The corresponding areas are denoted as A_{Ci}, A_{Con} and A_{Coex}. The total contrail area is $A_{totCon} := A_{Con} + A_{Coex}$. In order to focus on the contrail core, the analyses are additionally restricted to the 500 m deep layer below cruise altitude ($z = [1500\,\mathrm{m}, 2000\,\mathrm{m}]$). The corresponding areas are labelled A_{CiTop}, A_{ConTop} and $A_{CoexTop}$. The total top 500 m contrail area is then $A_{totConTop}$.

The same indices are used to denote the IC number in those areas ($\mathcal{N}_{Coex}$ or $\mathcal{N}_{totConTop}$, e.g.). In the co-existence area, ICs of both origins appear and a second index is used, if only ICs of a specific origin are counted. Then, e.g., $\mathcal{N}_{Coex,Ci}$ is the number of cirrus ICs in the co-existence area, whereas $\mathcal{N}_{totConTop,Con}$ is the number of contrail ICs in the top 500 m layer.

With this terminology it is possible to evaluate various ratios and their temporal evolution, for instance the contrail fractional area that contains co-existing

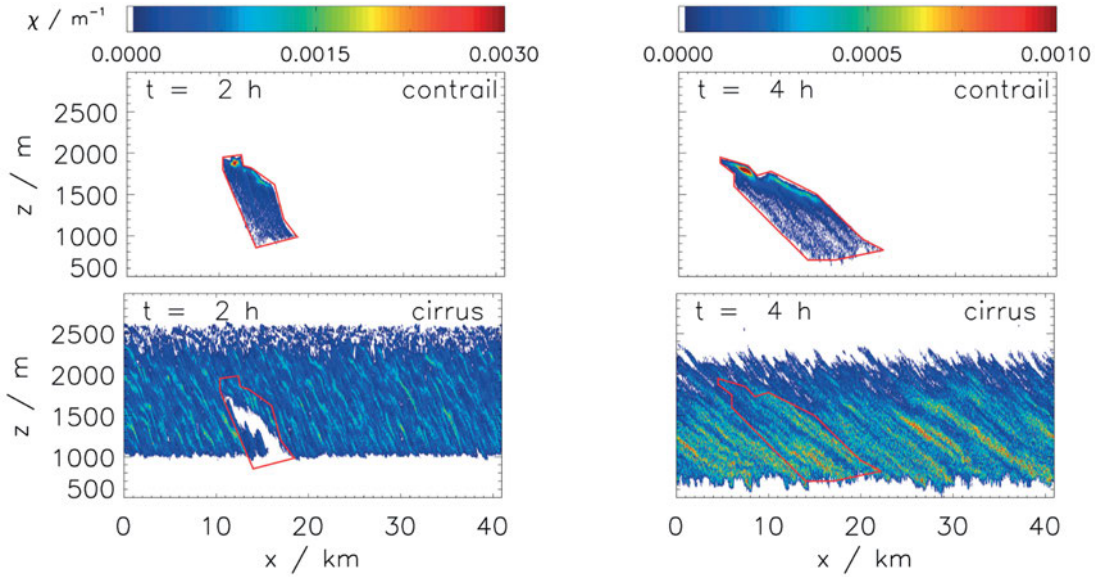

Figure 10: Extinction coefficient χ of either the contrail ice crystals only (top) or the cirrus ice crystals only (bottom), respectively for the indicated simulation time. The red polygons illustrate the contrail area. The ISS_up-simulation with $w_{syn} = 5\,\mathrm{cm\,s^{-1}}$ is depicted. Note the different ranges of the colour bars.

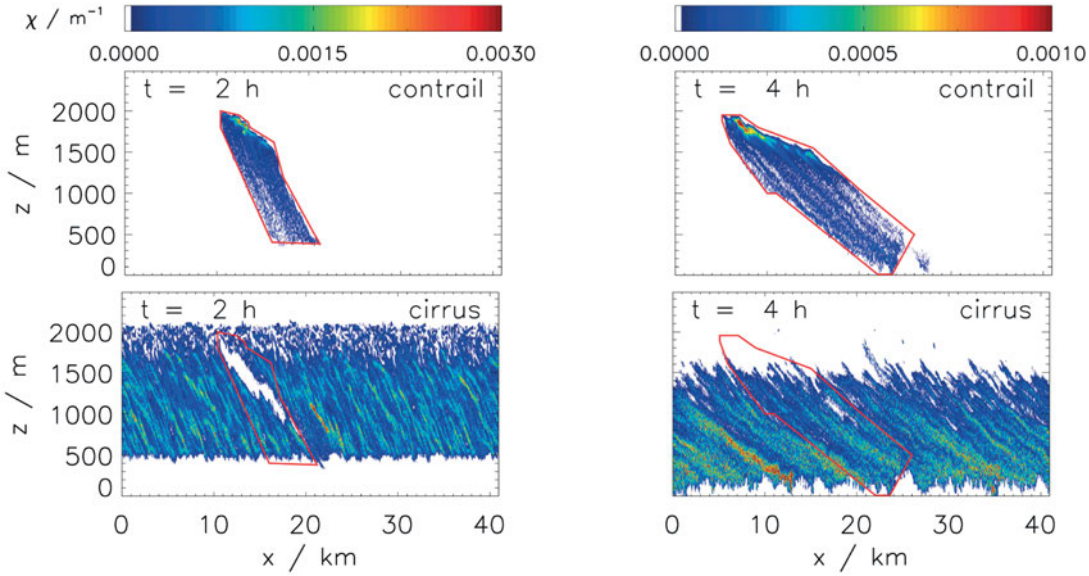

Figure 11: As Figure 10, but for the default simulation with $w_{syn} = 5\,\mathrm{cm\,s^{-1}}$. Note the different ranges of the colour bars.

cirrus ICs, $\eta_A = A_{Coex}/A_{totCon}$ (black curves in Figure 13) and the corresponding fraction of ICs, $\eta_N = \mathcal{N}_{Coex,Con}/\mathcal{N}_{totCon,Con}$ (red curves). Initially, there is only contrail and the co-existence fractions are zero. Once the cirrus forms at $t = 1$ h it takes around another two hours until η_A and η_N reach unity, meaning that the complete contrail is covered with cirrus ICs. This happens for contrails both at the top (solid lines) and in the middle (dotted) of the ISS layer. However, then they develop differently. For the contrail in the middle of the ISS layer, the co-existence fractions remain close to unity over many hours while the identity recovery for the contrail at the top of the ISS becomes manifested in the decreasing values of η_A and η_N.

Note that the extent of co-existence area depends on the resolution of the underlying mesh which implicitly determines the scale at which co-existence is rated. Our analyses use $10\,\mathrm{m} \times 10\,\mathrm{m}$-grid boxes. Even a larger contrail fraction would be classified as co-existence area, if a coarser resolution were used. Moreover, our analyses benefit from the low numerical diffusion of the Lagrangian microphysics which does not overestimate the IC mixing.

4.3 Alteration of properties by co-existence

Once cirrus ICs are mixed into a pre-existing contrail, the individual local properties of either get modified.

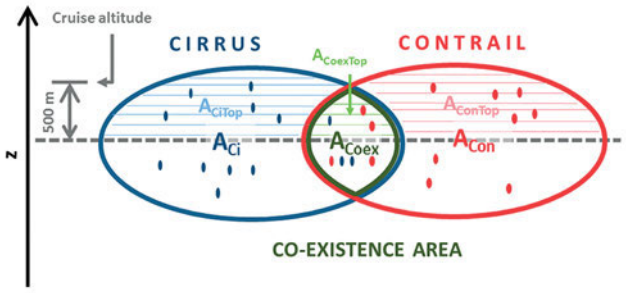

Figure 12: Sketch of the contrail, cirrus and the co-existence area. The areas of the pure contrail, the pure cirrus and co-existence area are denoted as A_{Con}, A_{Ci} and A_{Coex}, respectively. The corresponding areas restricted to the contrail upper part are called A_{ConTop}, A_{CiTop} and $A_{CoexTop}$. The total area of the contrail is denoted as A_{totCon}.

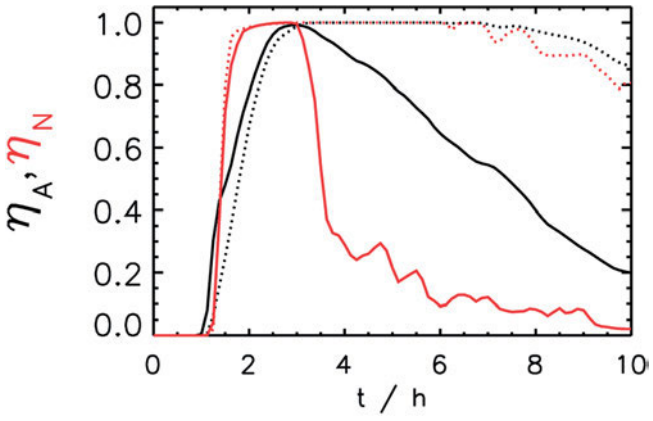

Figure 13: Contrail fraction with co-existing cirrus ice crystals relative to the total contrail, in terms of area $\eta_A = A_{Coex}/A_{totCon}$ (black) and ice crystal number $\eta_N = \mathcal{N}_{Coex,Con}/\mathcal{N}_{totCon,Con}$ (red). See text and Figure 12 for definitions of $A_?$ and $\mathcal{N}_?$. The solid/dotted curves show the default/ISS_up simulation with $w_{syn} = 5\,\mathrm{cm\,s^{-1}}$.

There are two components of such a change. First, all microphysical process rates are changed because the two IC populations compete for the excess WV. That is, initially growth rates are altered, and subsequently all other process rates, like sedimentation, are altered as a consequence. The impact of these changes on overall contrail properties like total extinction, average effective crystal diameter and total crystal number have been discussed above in Section 3.3. Second, even when the process rates would not change due to growth competition (for instance when there was saturation everywhere, such that growth rates were zero), the local properties of the combined cloud are different from the local properties derived from the contrails IC alone. Such analyses are relevant for the interpretation of in-situ measured contrails where methods like IC residue technique or chemical tracer analyses are available that can at least identify parts of contrails (see Section 4.2 in Unterstrasser et al., 2016). However, measurements inside contrails can be *contaminated* by an undetermined contribution of cirrus which can lead to qualitative changes. Some of these contamination effects are studied next. This will be done by first determining how many cirrus ICs are

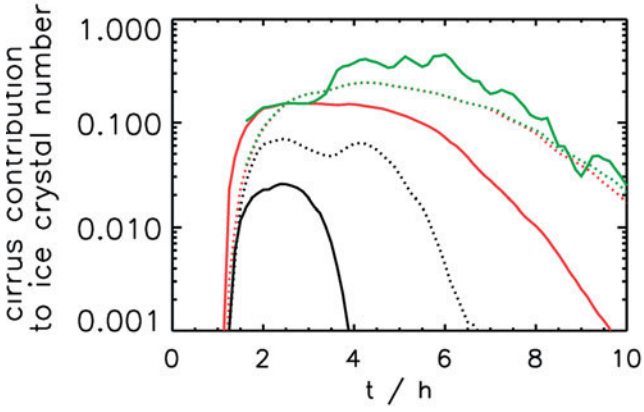

Figure 14: Relative cirrus contribution to the total ice crystal number $\mathcal{N}$ inside the contrail. Red: Cirrus $\mathcal{N}$ in co-existence area A_{Coex} relative to the total $\mathcal{N}$ (cirrus + contrail) in the complete contrail A_{totCon}. Green: Cirrus $\mathcal{N}$ in A_{Coex} relative to the total $\mathcal{N}$ in A_{Coex}. Black: Cirrus $\mathcal{N}$ in $A_{CoexTop}$ relative to the total $\mathcal{N}$ in the contrail upper part $A_{totConTop}$. The solid/dotted curves show the default/ISS_up simulation with $w_{syn} = 5\,\mathrm{cm\,s^{-1}}$.

typically present inside contrails. As an example, the results for the $w_{syn} = 5\,\mathrm{cm\,s^{-1}}$-simulations are depicted in Figure 14, both for the contrail at the top of the ISS layer (solid curves) and in the middle of the layer (dotted).

The following three ratios are computed:

1. the number of cirrus ICs in the co-existence area to the total number of ICs in the whole contrail area, $\mathcal{N}_{Coex,Ci}/\mathcal{N}_{totCon}$ (red curves),
2. the number of cirrus ICs to the total number of ICs in the co-existence area, $\mathcal{N}_{Coex,Ci}/\mathcal{N}_{Coex}$ (green curves), and
3. the same as in 2.), but for the top 500 m below flight altitude, i.e.$\mathcal{N}_{CoexTop,Ci}/\mathcal{N}_{CoexTop}$ (black curves).

Over the complete contrail (red curves), the cirrus contributes at most 25 % to the total number of ICs in the contrails (i.e. $\mathcal{N}_{Coex,Ci} < 0.25\ \mathcal{N}_{totCon}$). Hence, we find at least three times more contrail ICs than cirrus ICs in the contrail area. The cirrus contribution is larger when the contrail is in the middle of the cirrus instead of on top of it. If the analysis is restricted to the co-existence area (green curves), the share of the cirrus is larger and can make up around 40 %. The contrail core, roughly approximated by the top 500 m (black curves) is only little contaminated by cirrus ICs, even for the lower of the two contrails the cirrus fraction does not reach 10 % and for the higher contrail this value is rather a few percent.

Figure 15 (left and right column) displays various probability density functions (PDFs) of IC concentrations n for 2 h (top) and 4 h (bottom) after contrail formation. These PDFs refer to the complete contrail area (red), the co-existence area (green), and the top part of the contrail (black). The left column shows the PDFs of n irrespective of the crystal origin (i.e. both contrail and cirrus ICs, solid lines), while the right column shows the

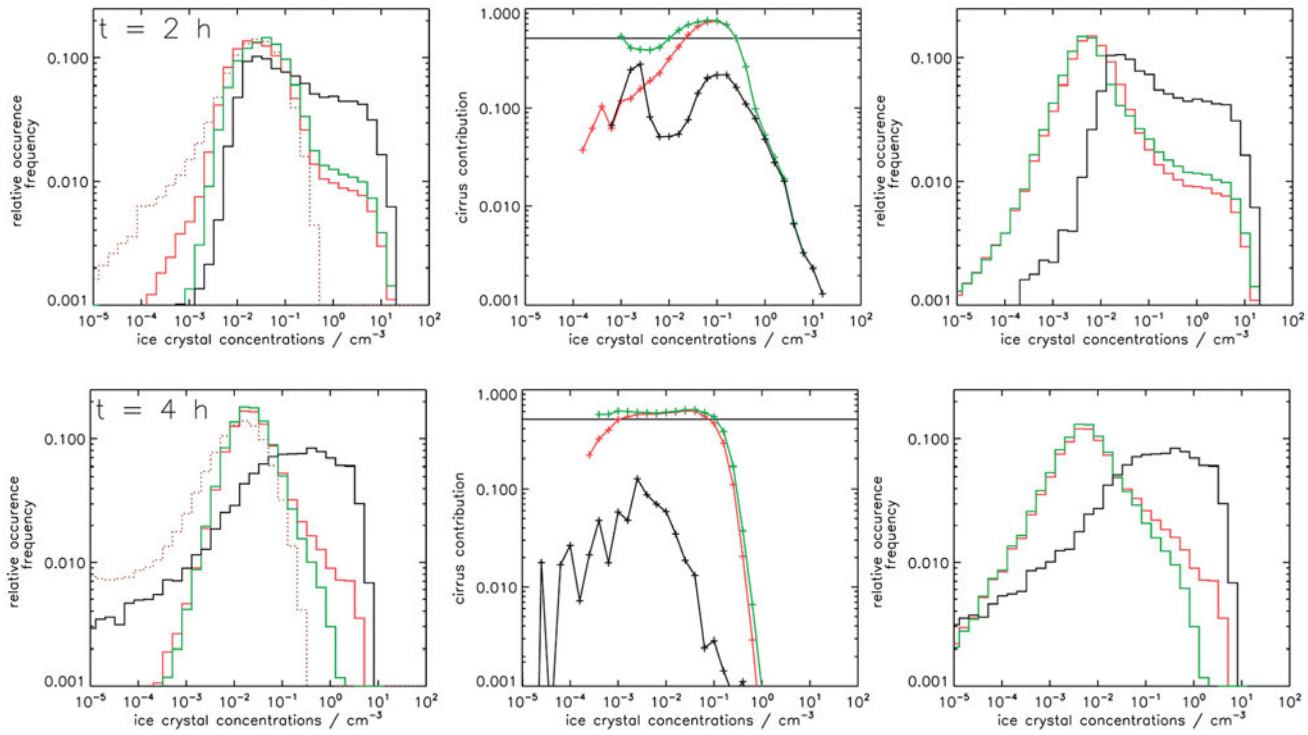

Figure 15: left: PDF of IC number concentrations n inside a certain area considering both cirrus and contrail ice crystals (IC). Middle: relative contribution of cirrus ICs to n in each n-bin. The horizontal line indicates the 50 %-line. Right: n-PDF inside a certain area considering only contrail ICs. As in Figure 14 the analyses are restricted to the complete contrail (red), the co-existence area (green) or the contrail upper part (black). The brown dotted histogram in the left column shows the n-PDF of the pure cirrus. In the PDF plots, the bin sizes increase exponentially. For each row, the displayed point in time is indicated in left-most column. The default simulation with $w_{syn} = 5\,\mathrm{cm\,s^{-1}}$ is depicted.

PDFs for contrail ICs only, where cirrus ICs are deliberately not counted in the computation of n in each grid box. To support the comparison of these PDFs, the middle row displays the cirrus ICs' share in each concentration interval. A further comparison can be made with the dotted curves in the left column which shows the PDFs of a pure cirrus (from a simulation without contrails from PART1 (Unterstrasser et al., 2016); cloud ages are the same).

Crystal concentrations vary over several orders of magnitude, with maximum values of the order $10\,\mathrm{cm^{-3}}$. Expectedly, these maxima are contributed by the contrail. Hence, the right tails of the PDFs in the left column (contrail + cirrus ICs) and the right column (only contrail ICs) are basically identical. The middle panels accordingly show the strongly decreasing cirrus share at high crystal concentrations. The most frequent concentrations of the pure cirrus (dotted curve) and the combined cloud (left column) are quite similar, of the order $10^{-1.5}\,\mathrm{cm^{-1}}$. The cirrus contribution to these mode values is quite large, exceeding 50 % (indicated by the horizontal black line in the middle panel). Not counting the cirrus contribution inside the contrail (right column), the most frequent concentrations are around one order of magnitude smaller, i.e. $10^{-2.5}\,\mathrm{cm^{-3}}$. Hence in this example, the cirrus ICs qualitatively change the PDFs of n measured inside contrails.

How the formation of a surrounding cirrus affects the size distribution (SD) of the embedded contrail has been shown above (cf. Figure 5) for the contrail ICs only. These were the changes brought about by the alteration of the microphysical process rates. However, mixing of the two crystal populations leads to qualitatively different changes in the size distributions, and these are considered next. Figure 16 shows for three situations with different updraught speed (columns) and for contrails at the top (top row) or in the middle of the moist layer (bottom row) the combined SDs (black dashed curves), which are superpositions of the contrail SDs (red solid curves, the same as in Figure 5) and the SDs of co-existing cirrus (blue solid curves). The blue dotted curves show the SDs of the total cirrus (i.e. including contrail and contrail-free areas).

The latter, that is the SD of the whole cirrus, tends in all cases to a bimodal shape, with a weak sublimation tail at small crystal sizes and a main mode at sizes ranging from 40 µm to about 100 µm. The pure contrail SD is bimodal as well, but with a main mode at small sizes and a secondary accumulation mode (fall streak) as already reported in PART1 (Unterstrasser et al., 2016) . In this sense, these SDs are mirror images of each other, and the combined size distribution features a prominent bimodality with two strong local maxima, the one at smaller sizes due to the contrail contribution,

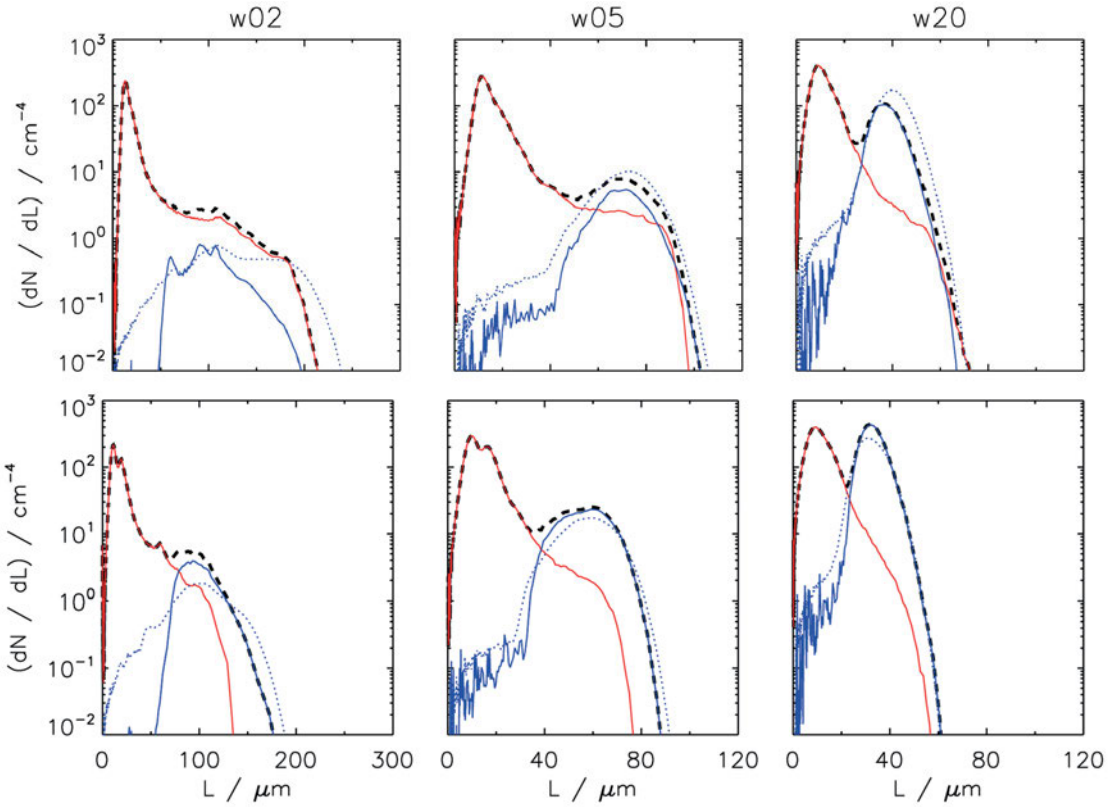

Figure 16: Size distribution of all ice crystals (black dashed), contrail ice crystals only (red) or cirrus crystal only (blue solid) inside 4 hour contrails. Analogous to the total and the contrail SD, the cirrus SD is averaged over the total contrail area, even though cirrus ice crystals may not cover the complete contrail. Then the black curve is the superposition of the red and blue curve. The SD of the complete cirrus (blue dotted) is given for comparison (here the average is taken over the cirrus area). The top/bottom row shows the default/ISS_up simulations for the indicated updraught speeds. Note the different ranges of the x-axes in the various columns.

the one at the larger sizes contributed by the cirrus. The cirrus contribution increases with increasing updraught speed. It is very weak in the slow uplift cases; an even weaker uplift would probably not suffice to produce a true second maximum in the SD. In the ISS_up case, the contrail ICs in the smaller fall streak do not grow as large as in the default case, thus the cirrus ICs substantially contribute to the $L > 80\,\mu$m IC population.

Microphysical properties measured in contrails (as exemplified for PDFs of n and SDs) can be contaminated by co-existing ICs. The few analysed examples show already a large range of possible modifications. The direction and size of any modification depend on the respective situation which makes it difficult to abstract generally valid conclusions of such an interaction from the simulations. But sometimes indications for an interaction can be found. Kübbeler et al. (2011) measured large ICs in young contrail cores, which could not be explained by contrail-intrinsic processes. Hence, they concluded that those ICs originate from cirrus aloft. Our findings support their interpretation of the contrail observation.

5 Discussion

Anticipating the complexity of the problem we tried to keep the simulations for this paper relatively simple by deliberately switching off certain processes like heterogeneous nucleation, radiation and aggregation. This section discusses what can be expected if these simplifications would not have been made.

Probably the most serious simplification is to neglect heterogeneous nucleation. Cirrus measurements in the INCA experiment (Interhemispheric Differences in Cirrus Properties From Anthropogenic Emissions; http://www.pa.op.dlr.de/inca and Ström et al., 2003) showed that cirrus formation in the northern mid-latitudes is probably always influenced by heterogeneous nucleation. In fact, one of the questions driving INCA was whether naturally formed cirrus (i.e. formed purely by homogeneous nucleation) does exist at all at northern mid-latitudes. Ice nuclei (IN, e.g. soot) originating from aviation itself but also from industrial emissions occur in cruise altitudes in the northern hemisphere and it is probable that they affect cirrus formation (Ström and Ohlsson, 1998; Haag et al., 2003; Sölch and Kärcher, 2011). The large land masses of the northern mid-latitudes provide additionally mineral dust particles serving as heterogeneous IN. We must accept therefore that probably most aviation takes place in regions that are polluted by anthropogenic emissions and where IN of natural origin occur. In spite of that we decided to make the idealistic assumption that cirrus formation is not influenced by heterogeneous nucle-

ation. This was to our view necessary and justified. It was necessary to keep the complexity of the simulation tractable and it was justified because heterogeneous nucleation does not exclude later homogeneous nucleation (Gierens, 2003) and when this happens, cirrus clouds are still often dominated by ICs formed homogeneously (Spichtinger and Gierens, 2009a).

Heterogeneous ice formation can proceed at lower supersaturations than homogeneous nucleation, but it leads to cirrus with low crystal concentrations, that is, thin cirrus. For the present problem this means on one hand that the time span t_{age} between contrail and cirrus formation would be reduced and the contrail confinement would start earlier, but on the other hand the confinement would be weaker. Should homogeneous nucleation set in at a later time, it would only lead to lower crystal concentrations because the pre-existing heterogeneously formed ICs retard the rate at which the supersaturation changes at the nucleation threshold (Spichtinger and Gierens, 2009a). Heterogeneous nucleation can even inhibit later homogeneous nucleation when the pre-existing ICs have a concentration that suffices to consume excess vapour faster than it is replaced by further uplift (that is, when their deposition time scale is smaller than the updraught time scale). In such case, a purely heterogeneously formed thin cirrus would surround the contrail and the contrail might stand out as a very strong peak in 2D maps of number concentration, extinction and lidar backscatter. It is conceivable that the lidar measurement displayed in Figure 6 shows just such a case. There is much larger (factor ten) contrast between several "hot spots" in backscatter than in the extinction maps of the simulations with homogeneously nucleated cirrus only. However, this is just speculation. It seems impossible to make general predictions on the possible behaviour of the contrail's total extinction, for instance, should there be both types of cirrus formation; too large are the possible ranges of critical supersaturation and ice nucleus number concentrations.

Another simplification is the disregard of aggregation. ICs in the contrail core have very small fall speeds, but cirrus ICs, formed above the contrail core can grow large enough in their supersaturated environment to attain fall speeds of several 10 cm s^{-1}. Gierens (2012) estimates that such a cirrus can collect a considerable number of contrail core ICs after a few hours, thus enhance the erosion of the contrail core and reduce possibly the contrail lifetime. This requires that there is a continuous source of falling ICs above the contrail core during a couple of hours which is only possible in a continuous updraught with recurrent nucleation events at the upper part of the ISS layer. The thickness of the ISS layer may play a role in this case. While our simulations showed similar results for a thinner and a thicker ISS layer, with similar d_{down} in both cases, the smaller or larger source of falling ICs potentially produces differences in the contrail a few hours after cirrus formation.

Radiation effects can be strong in contrails (Unterstrasser and Gierens, 2010b; Lewellen, 2014), in particular under weakly stratified conditions, on sunny summer days without other clouds. Lower, mid-level clouds and cirrus below a contrail weaken the infrared irradiance entering the contrail. Cirrus above the contrail can emit long-wave downward radiation of much higher intensity than the clear atmosphere. This is an energy source for the contrail. The effect of cirrus around a contrail is thus probably a complex one, depending on the details of the situation. Studies of such effects deserve an investigation on its own and are therefore beyond the scope of the present paper.

Finally, we have not considered the case where a contrail is formed within an already existing cirrus. This may be a quite frequent situation since pilots usually do not circumvent the passage of cirrus clouds. A few simple questions concerning this case have been treated analytically elsewhere (Gierens, 2012). For a general treatment, a new class of simulations would have to be performed. This is beyond the horizon of the present paper.

Contrail and cirrus evolution is affected by many more parameters (stratification, temperature, aircraft parameters, radiation-related parameters, nucleation mechanism), which we did not vary in this study. Already the modest range of investigated parameter settings produces a diversity of phenomena due to a complex interaction of contrails and cirrus. The selected scenarios give merely a first impression of what is possible.

The simulations of PART1 (Unterstrasser et al., 2016) demonstrated that different parameters are important for contrails on one hand and cirrus on the other hand. The present simulations show additionally that both cloud types undergo a complex interaction and compete for the available WV. This can cause nonlinear effects on instantaneous radiative forcing (RF) values. Hence, approaches in large scale models that consider a separate contrail cloud class, the feedback with the hydrological cycle and the competition for the available WV (Burkhardt and Kärcher, 2009; Schumann et al., 2015; Bock and Burkhardt, 2016) have to be preferred over approaches where the contrail modifies only the cirrus cloud class (Chen et al., 2012) or contrails are treated offline (Schumann, 2012).

6 Conclusions

The Lagrangian ice microphysical module LCM together with the flow solver EULAG has been used to perform simulations of contrail-cirrus interacting with natural cirrus formed by homogeneous nucleation after contrail formation. For this, idealised scenarios with constant updraught speed (i.e. cooling rates) over a certain period of time were used, where cirrus forms around a pre-existing contrail. Such scenarios are compared to scenarios, where the ascent stops, before natural cirrus formation sets in and contrails evolve in an unperturbed manner. We first formulated several theoretical expectations and then examined the simulation results.

We find that in high updraught scenarios, where cirrus forms shortly after the contrail generation, the contrail spreading is inhibited by the surrounding cirrus and contrail total extinction is strongly reduced compared to a contrail in clear sky. In particular, the development of a strong fall streak is hampered and large contrail ice crystals (IC) are less abundant than in an unperturbed contrail. In a slow updraught, cirrus forms later around a mature contrail and the contrail's further evolution is not considerably constrained by the cirrus. In a sensitivity study, the contrail formation altitude was shifted from the top to the middle of a 1200 m deep ice supersaturated (ISS) layer. Clearly, the emerging fall streak is smaller and the contrail total extinction is smaller compared to the default case. Moreover, the effect of a surrounding cirrus is not as strong, as the contrail development is anyway limited due to the shallower ISS layer below the contrail. The effective crystal diameters of unperturbed contrails increase within the first 1–2 hours and then reach a quasi-constant value of 50 µ–60 µm for contrails at the top or of < 40 µm for contrails in the middle of the ISS layer. Once cirrus forms around a contrail, the contrail effective diameter starts to decrease with time and much smaller effective diameters around 20 µm can occur. Moreover, the contrail ice crystal number loss due to sedimentation is decelerated by surrounding cirrus, as ice crystal growth at the contrail periphery is slowed down and fewer ICs fall out.

We analyse the extinction coefficient as a proxy of the lidar backscatter ratio as measured for instance by airborne lidars. Although there are qualitative differences between the real lidar curtain (Figure 6) and our proxies from the idealised scenarios, we see that it can be difficult to identify a contrail as such once it is embedded in a thick natural cirrus. This even turned out difficult when the simulated cirrus was less strong (slower updraught cases). Moreover, we find situations where internal dynamics lead to natural cirrus fields that contained band-like structures that resemble the shape of contrails. It might be easier to identify embedded contrails in cirrus clouds that are thin (low crystal concentration) either because of very slow updraught or because of a dominance of heterogeneous nucleation or both.

We further demonstrate that cirrus ICs exist in large parts of the contrail. Mainly, differential sedimentation leads to their co-existence. Cirrus ICs overtake smaller contrail ICs, particularly in the contrail core. ICs in the contrail fall streak can be larger than those of the surrounding cirrus and the fall streak penetrates into the cirrus. An only 100–200 m thick cirrus layer above the contrail suffices to produce enough ICs such that eventually the whole contrail is populated with cirrus ICs. If the contrail is located in the middle of the ISS layer and a much thicker cirrus lies above the contrail, this state of complete contrail "contamination" can persist over several hours. These findings imply that a strict separation into a cirrus area, on the one hand, and a contrail area, on the other hand may not be meaningful. Aggregation (which we neglected in this study) may produce aggregates with mixed origin, that is, even single ICs could not be attributed to a unique source. We must accept that in such cases the two crystal populations are so intimately connected that it is no longer possible and moreover no longer meaningful to separate their effects on radiative forcing, for instance.

We found that one fourth of all ICs inside a specific contrail were of natural origin. In the contrail core, where most of the contrail ICs reside, the cirrus contribution to the total ice number is less than 10 %. The microphysical properties computed from all ICs in a contrail can be perturbed by the co-existing cirrus ICs, e.g. size distributions feature a second "cirrus" mode. The cirrus signature is more pronounced, when the updraught is stronger (i.e. the cirrus forms earlier and has higher number concentration) and/or the contrail is in the lower part of the ISS layer.

The theoretical considerations and the idealised simulations both indicate a large degree of variability in the interaction of pre-existing contrails with later forming cirrus. The situation is even much more involved in nature, where processes like heterogeneous nucleation, aggregation and radiation are not "switched off", where updraught is controlled by synoptic-scale dynamics, where medium-scale dynamics leads to much more medium-scale (say 10–20 km) structure in the cirrus than in our simulations, where also contrails can be formed within pre-existing cirrus of various types, and where many contrails may interact in regions with dense air traffic. All this shows that the interaction of contrail-cirrus and natural cirrus is a tremendously large field of research in which we have just scratched the surface. Much remains to be done.

Acknowledgements

The first author S. Unterstrasser is partly funded by the DFG (German Science Foundation, contract number UN286/1-2). Computational resources were made available by the German Climate Computing Center (DKRZ) through support from the German Federal Ministry of Education and Research (BMBF). The work contributes to the DLR project WeCare. We thank K. Graf for comments on the manuscript.

References

Bock, L., U. Burkhardt, 2016: The temporal evolution of a long-lived contrail cirrus cluster: Simulations with a global climate model. – J. Geophys. Res. **121**, 3548–3565, DOI: 10.1002/2015JD024475.

Burkhardt, U., B. Kärcher, 2009: Process-based simulation of contrail cirrus in a global climate model. – J. Geophys. Res. **114**, D16201, DOI: 10.1029/2008JD011491.

Burkhardt, U., B. Kärcher, 2011: Global radiative forcing from contrail cirrus. – Nature Climate Change **1**, 54–58.

Chen, C., A. Gettelman, C. Craig, P. Minnis, D. Duda, 2012: Global contrail coverage simulated by CAM5 with the inventory of 2006 global aircraft emissions. – J. Adv. Model. Earth Syst. **4**, DOI: 10.1029/2011MS000105.

Dobbie, S., P. Jonas, 2001: Radiative influences on the structure and lifetime of cirrus clouds. – Quart. J. Roy. Meteor. Soc. **127**, 2663–2682, DOI: 10.1002/qj.49712757808.

Dürbeck, T., T. Gerz, 1995: Large-eddy simulation of aircraft exhaust plumes in the free atmosphere: effective diffusivities and cross-sections. – Geophys. Res. Lett. **22**, 3203–3206.

Gierens, K., 2003: On the transition between heterogeneous and homogeneous freezing. – Atmos. Chem. Phys. **3**, 437–446.

Gierens, K., 2012: Selected topics on the interaction between cirrus clouds and embedded contrails. – Atmos. Chem. Phys. **12**, 11943–11949.

Haag, W., B. Kärcher, J. Ström, A. Minikin, U. Lohmann, J. Ovarlez, A. Stohl, 2003: Freezing thresholds and cirrus cloud formation mechanisms inferred from in situ measurements of relative humidity. – Atmos. Chem. Phys. **3**, 1791–1806.

Heymsfield, A., R. Lawson, G. Sachse, 1998: Growth of ice crystals in a precipitating contrail. – Geophys. Res. Lett. **25**, 1335–1338.

Koenig, L., 1971: Numerical Modeling of Ice Deposition. – J. Atmos. Sci. **28**, 226–237.

Kübbeler, M., M. Hildebrandt, J. Meyer, C. Schiller, T. Hamburger, T. Jurkat, A. Minikin, A. Petzold, M. Rautenhaus, H. Schlager, U. Schumann, C. Voigt, P. Spichtinger, J.-F. Gayet, C. Gourbeyre, M. Krämer, 2011: Thin and subvisible cirrus and contrails in a subsaturated environment. – Atmos. Chem. Phys. **11**, 5853–5865, DOI: 10.5194/acp-11-5853-2011.

Lewellen, D.C., 2014: Persistent contrails and contrail cirrus. Part 2: Full Lifetime Behavior. – J. Atmos. Sci., published online, 4420–4438, DOI: 10.1175/JAS-D-13-0317.1.

Lewellen, D.C., O. Meza, W.W. Huebsch, 2014: Persistent contrails and contrail cirrus. Part 1: Large-eddy simulations from inception to demise. – J. Atmos. Sci., published online, 4399–4419, DOI: 10.1175/JAS-D-13-0316.1.

Liu, H., P. Wang, R. Schlesinger, 2003: A Numerical Study of Cirrus Clouds. Part II: Effects of Ambient Temperature, Stability, Radiation, Ice Microphysics, and Microdynamics on Cirrus Evolution. – J. Atmos. Sci. **60**, 1097–1119.

Mitchell, D., 1996: Use of mass- and area-dimensional power laws for determining precipitation particle terminal velocities. – J. Atmos. Sci. **53**, 1710–1723.

Schumann, U., 2012: A contrail cirrus prediction model. – Geosci. Model Dev. **5**, 543–580, DOI: 10.5194/gmd-5-543-2012.

Schumann, U., J.E. Penner, Y. Chen, C. Zhou, K. Graf, 2015: Dehydration effects from contrails in a coupled contrail-climate model. – Atmos. Chem. Phys. **15**, 11179–11199, DOI: 10.5194/acp-15-11179-2015.

Smolarkiewicz, P., L. Margolin, 1997: On Forward-in-Time Differencing for Fluids: an Eulerian/Semi-Lagrangian Non-Hydrostatic Model for Stratified Flows. – In: Lin, C., R. Laprise, H. Ritchie (Eds.): Numerical Methods in Atmospheric and Oceanic Modelling: The André J. Robert Memorial Volume **35**. – Canadian Meteorological and Oceanographical Society, Ottawa, Canada, 127–152.

Smolarkiewicz, P., L. Margolin, 1998: MPDATA: A Finite-Difference Solver for Geophysical Flows. – J. Comput. Phys. **140**, 459–480.

Sölch, I., B. Kärcher, 2010: A large-eddy model for cirrus clouds with explicit aerosol and ice microphysics and Lagrangian ice particle tracking. – Quart. J. Roy. Meteor. Soc. **136**, 2074–2093.

Sölch, I., B. Kärcher, 2011: Process-oriented large-eddy simulations of a midlatitude cirrus cloud system based on observations. – Quart. J. Roy. Meteor. Soc. **137**, 374–393.

Spichtinger, P., K. Gierens, 2009a: Modelling of cirrus clouds – Part 2: Competition of different nucleation mechanisms. – Atmos. Chem. Phys. **9**, 2319–2334.

Spichtinger, P., K.M. Gierens, 2009b: Modelling of cirrus clouds - Part 1a: Model description and validation. – Atmos. Chem. Phys. **9**, 685–706.

Ström, J., S. Ohlsson, 1998: In situ measurements of enhanced crystal number densities in cirrus clouds caused by aircraft exhaust. – J. Geophys. Res. **103**, 11355–11361.

Ström, J., M. Seifert, B. Kärcher, J. Ovarlez, A. Minikin, J.-F. Gayet, R. Krejci, A. Petzold, F. Auriol, W. Haag, R. Busen, U. Schumann, H. Hansson, 2003: Cirrus cloud occurrence as function of ambient relative humidity: A comparison of observations obtained during the inca experiment. – Atmos. Chem. Phys. **3**, 1807–1816.

Unterstrasser, S., 2014: Large eddy simulation study of contrail microphysics and geometry during the vortex phase and consequences on contrail-to-cirrus transition. – J. Geophys. Res. **119**, 7537–7555, DOI: 10.1002/2013JD021418.

Unterstrasser, S., K. Gierens, 2010a: Numerical simulations of contrail-to-cirrus transition – Part 1: An extensive parametric study. – Atmos. Chem. Phys. **10**, 2017–2036.

Unterstrasser, S., K. Gierens, 2010b: Numerical simulations of contrail-to-cirrus transition – Part 2: Impact of initial ice crystal number, radiation, stratification, secondary nucleation and layer depth. – Atmos. Chem. Phys. **10**, 2037–2051.

Unterstrasser, S., N. Görsch, 2014: Aircraft-type dependency of contrail evolution. – J. Geophys. Res. **119**, 14,015–14,027, DOI: 10.1002/2014JD022642

Unterstrasser, S., I. Sölch, 2014: Optimisation of simulation particle number in a Lagrangian ice microphysical model. – Geosci. Model Dev. **7**, 695–709, DOI: 10.5194/gmd-7-695-2014.

Unterstrasser, S., K. Gierens, I. Sölch, M. Lainer, 2016: Numerical simulations of homogeneously nucleated natural cirrus and contrail-cirrus. Part 1: How different are they? – Meteorol. Z., DOI:10.1127/metz/2016/0777.

Wirth, M., A. Fix, P. Mahnke, H. Schwarzer, F. Schrandt, G. Ehret, 2009: The airborne multi-wavelength water vapor differential absorption lidar wales: system design and performance. – Applied Physics B **96**, 201–213, DOI: 10.1007/s00340-009-3365-7.